Measurement of Muon Performance and Determination of Z Boson Production Cross Section using CMS Detector at LHC

By

Aleena Rafique

SUBMITTED IN PARTIAL FULFILLMENT OF THE
REQUIREMENTS FOR THE DEGREE OF
MASTER OF PHILOSOPHY
AT
DEPARTMENT OF PHYSICS
QUAID-I-AZAM UNIVERSITY, ISLAMABAD
JUNE 2013

Certificate

The undersigned hereby certify that they have read and recommend to the Department of Physics for acceptance of thesis entitled "**Measurement of Muon Performance and Determination of Z Boson Production Cross Section using CMS Detector at LHC**" by **Aleena Rafique** in partial fulfillment of the requirements for the degree of **Master of Philosophy**.

Supervisor:

Prof. Dr. Hafeez Hoorani
Director Research
National Center for Physics
Islamabad, Pakistan

Submitted Through:

Prof. Dr. Muhammad Zakaullah
Chairman
Department of Physics
Quaid-i-Azam University
Islamabad, Pakistan

QUAID-I-AZAM UNIVERSITY

Date: **JUNE 2013**

Author: **Aleena Rafique**

Title: **Measurement of Muon Performance and Determination of Z Boson Production Cross Section using CMS Detector at LHC**

Department: **Physics**

Degree: **MPhil**

Signature of Author

To My Beloved Parents .

"Every bit of me is a little bit of you"

Acknowledgements

In the name of ALLAH, the Most Merciful, Most Gracious, and Benevolent. I glorify Almighty ALLAH for his countless blessings and send salutations to his last Prophet Muhammad (PBUH) whose favours are the sole cause for enabling me to accomplish the tedious job of furnishing my research work. May Allah's peace and blessing be upon our Beloved Prophet Muhammad (PBUH) who is the seal of the prophets, and on his pure and pious progeny.

I take this opportunity with pride and enormous gratification to express the feelings of gratefulness from the bottom of my heart to all the persons who backed me directly or indirectly throughout the materialization of this research work at this magnitude, without which this thesis might not have been written, and to whom I am greatly indebted.

First and the foremost, I deem it a rare opportunity to pronounce my deep sense of gratitude to my venerable teacher and supervisor, Prof. Dr. Hafeez Hoorani, who has the attitude and the substance of a genius: he continually and convincingly conveyed a spirit of adventure in regard to research-knowing when to push and when to let up. I am very thankful to him for his direction and help in the development of my scientific mind. His kind behaviour, encouraging nature and inspiring attitude made it very easy for me to understand precisely and perform accurately this work throughout the period of research.

I am also highly indebted to pay my heartiest gratitude to Dr. Ashfaq Ahmad for his valuable and constructive guidance and assistance throughout the planning, development and accomplishment of this research work. His willingness to give his time so generously has been very much appreciated. I always could rely on his remarkable ability to sense and distil any problem so quickly. His patience and considerate nature made him accessible whenever I needed his assistance. Without his guidance and persistent help this dissertation would not have been possible.

With great pleasure, I would like to thank Prof. Dr. Muhammad Zakaullah, Chairperson, Department of Physics, Quaid-i-Azam University, Islamabad for providing me the opportunity and facilities to work in this esteemed institute and for allowing me to do research work at NCP.

I would like to thank my parents, Chuhadry Muhammad Rafique and Aalia Rafique, for not only raising and nurturing me but also for their unconditional support, both financially and emotionally over the years for my education and intellectual development. I am heartily thankful to you for the myriad of ways in which, throughout my life, you have actively supported me in my determination to find and realize my potential, and to make this contribution to our world. A very special thank you for providing a writing space and for nurturing me through the months of writing and showing your care and support in incredible ways.

To my aunt, Naz Khushi Muhammamd, who represented to me living proof of women′s ability to redefine and recreate our lives and who has given me her unequivocal support throughout, as always, for which my mere expression of thanks likewise does not suffice.

It is also dedicated to my siblings Khezina, Khaqan and Rohan for their encouragement and moral support throughout whole of this work especially through their insightful comments and hard questions.

I greatly acknowledge EHEP group members at NCP, who made a friendly environment for working. Encouragement and Support by Dr. Shamoona Fawad Qazi, Dr. Jamila Bashir Butt, Dr. Irfan Asghar, Ahmad Bhai, Taimoor bhai, Wajid bhai, Qamar bhai, Izhar bhai, Gul bhai, Qasim bhai, Bilal, Zeeshan, Atif, Athar bhai, Shawana, Fakhra, Tahira and Sobia made possible for me to work comfortably in EHEP group.

Loving thanks to my friends at QAU Sidra, Saira, Huma, Kanza, Ameena, Tayyaba, Tahira, Kasifa, Nosheen and Noor ul ain, who played such important roles along the journey, as we mutually engaged in making sense of the various challenges we faced and in providing encouragement to each other at those times when it seemed impossible to continue.

Despite these acknowledgements, the weaknesses and limitations of this thesis remain all mine.

Aleena Rafique

Abstract

This dissertation presents the measurement of production cross section of Z boson through Z→ $\mu^+\mu^-$ at $\sqrt{s}$ = 8 TeV using 2012 data recorded by CMS detector at LHC. The full dataset (DoubleMu Run A) having integrated luminosity of 0.82 fb^{-1} was analysed. Performance of muons reconstructed in CMS detector was studied by measuring identification efficiencies using data driven tag and probe method. Muon resolution reconstruction was studied by comparing dimuon mass resolution in data and MC. The impact of muon momentum scale and resolution correction and kinematic distribution is also reported in thesis. The measured Z boson cross section in dimuon channel is "σ_{prod} = 1.17±0.06 (stat,lumi) nb" which is found in agreement with the published CMS results.

Table of Contents

List of Tables

List of Figures

Chapter 1

Theoretical Overview

Switzerland is known to be the “Paradise on Earth”. The paradise is defined to be the place where nature lives and is famous because of its natural beauty. So one can assume that Switzerland is the country enrich with the natural beauty but beneath the land of this country, the world’s largest machine “Large Hadron Collider” (LHC) is running. So here is a contradiction but by observing the matter closely, we come to know that the purpose of this machine is the search of nature (origin of earth) and it is our thinking that we can find some clues about the ‘origin of earth’ from the ‘paradise on earth’. So basically, we are in search of ‘nature’ by using ‘artificial’ means in the ‘natural’ environment.

As we know that heat always travels from hot to cold body hence it is unidirectional and according to “second law of thermodynamics”, we have to do some extra amount of work if we want to transfer heat from cold to hot reservoir. As time is also unidirectional so by applying above mentioned law for the time zone, we can say that we have to do a lot of work in order to go back in time. That work is done normally by using some artificial means e.g in our case we use LHC machine for this purpose.

By using complex machine e.g LHC, we are basically interested to know that how complex the nature could be.

- **Complexity of the Nature**

When we move towards the basic unit of matter, we actually move towards the 'Complexity of the Nature' e.g we come to know that there are many types of fundamental particles that exist in nature so one can imagine that what could be the actual form of nature and how complex it could be. It could be the way beyond one's (human) imagination but it is our responsibility to test our knowledge and search for these mysteries so that we might be able to atleast touch the surface of revelation.

High Energy Physics Theorists have made some efforts for that purpose in the form of Standard Model of Particle Physics (SM) which governs the behaviour of fundamental particles and the interaction present among them. The experimentalists also go hand in hand with the theory in discovering particles predicted by the theory. Recently, by finding Higgs like boson, experimentalists have found the last missing particles to be discovered from the Standard Model.

As achieving a goal gives us a 'self confidence' that we were moving in right direction plus a 'motivation' and 'stimulation' that we can also be successful in achieving somewhat much more complex task.

Also as we moved from "Classical Physics" to "Modern Physics" in the start of 20^{th} century so now we expect to go to some "Ultra Modern Physics" or what we call it a "New Physics" which deals with many more mysteries and complexities.

1.1 High Energy Physics (HEP)

The study of High Energy Physics, also known as Particle Physics, grew out of nuclear and cosmic ray physics in the 1950's, and measured the properties and interactions of fundamental particles at the highest energies (millions of electron-volts) then available with a relatively new technology, particle accelerators. Today we have achieved that goal and we can even produce controlled beams having trillions of electron-volts energy. With the help of this, we are able to look into matter more closely and now we can probe the smallest dimensions of matter and even can tell about the very early history of our universe.

Basically the goal of High Energy Physics is to understand how forces and particles of our universe merge together into a single picture, the search of new space-time dimensions and the search of mysterious particles and forces that have created indelible imprints on our universe.

1.2 The Standard Model of Particle Physics

As nature has placed almost every thing in a perfect order or arrangement. It's been very interesting search for scientists and philosophers to look for that 'Model', on the basis of which other things can be described easily. In case of atomic structure, a model was needed which will describe the matter in true sense. First effort called ta atoma [1] was made by ancient Greek philosophers in this respect but it was rather more philosophic than scientific approach. In 1904, Joseph Thomson, first published the so-called Plum Pudding Model [2] but this model was not able to explain light spectra of atoms. Rutherford then improvised that model describing electrons orbiting around the nucleus but it also had some flaws i.e electron continuously radiating energy. Then Neil Bohr explained the true structure of atom i.e electrons orbiting around nucleus in fixed orbits.

1.2.1 Constituents of Standard Model

Today, by achieving very high energies of the probing particles using colliders, we are now able to look further into the atom, nucleus and even in proton and neutron. The collective model having fundamental particles (known to us up till by now) and the interactions between them is said to be the 'Standard Model of Particle Physics.'

The main constituents of Standard Model are Intermediate vector bosons, fermions and fundamental forces and their interactions. Now we will describe these in details.

Intermediate Vector Bosons

Vector boson is a boson having spin quantum number equal to '1'. These are the force carriers of different fundamental interactions. In standard model, we deal with intermediate vector gauge bosons which have various parameters as described in following table (1.1).

Table 1.1: gauge bosons in SM and various parameters: quantum number J^P, charge q and of weak isospin third component T_3

Bosons	Interaction	Mass	J^P	q	T_3
γ	electro.mag	-	1^-	0	0
Z^0	weak	91.18 GeV/c^2	1	0	0
$W^\pm$	weak	80.40 GeV/c^2	1	$\pm e$	± 1
8 $Gluons(g)$	strong	-	1^-	0	0

Fermions

Beside these gauge bosons, twelve fundamental particles are divided into two groups i.e quarks and leptons (see Table 1.2). These fundamental particles are called *Fermions*. These particles have half integer spin, obey Pauli′s Exclusion Principle and each of these particles can be grouped into three generations or families. Antiparticle of every particle have exactly same mass but other quantum numbers are opposite.

Table 1.2: The fundamental fermions

Fermion	Generation 1	2	3	charge	weak isospin	color
Leptons	ν_e	ν_μ	ν_τ	0	+1/2	-
	e	μ	τ	-e	-1/2	-
Quarks	u	c	t	+2/3e	+1/2	r,b,g
	d'	s'	b'	-1/3e	-1/2	

These fermions are arranged in pair into three families in form of isospin doublets. The ‘prime’ with quarks indicate that mass eigenstates of these quarks are not same as the weak interaction eigenstates.

These are further divided into two types, leptons and quarks.

- **Leptons**

  Leptons are the fermions which do not participate in strong interactions. These generally cannot be seen into a nucleus. There are three lepton flavours. Six leptons in total exist according to SM i.e electron (e), muon (μ), tau (τ) and their respective neutrinos. Each lepton also have a corresponding neutrino (e.g electron neutrino). Only one helicity[3] is observed for the neutrino (neutrinos are left-handed). Each lepton also have an antiparticle (antineutrinos are right-handed).

- **Quarks**

  The term ‘quark’ was first introduced by Murray Gell-Mann. Quarks are fermions which can interact through all four fundamental forces. There are six flavours of quarks which are arranged into three generations i.e up (u) & down (d), charm (c) & strange (s), top (t) & bottom (b). Antiparticles of quarks are called ‘antiquarks’.

- **Composite subatomic Particles**

  We can never have a quark in isolated form. It is always found in the combined form. These combined particles are called as "Composite Subatomic Particles". We find quarks as fundamental particles in composite particles called 'Hadrons'.

- **Hadrons**

  Hadrons are multiple quarks bound together through strong interaction. It can exists into bound form of either three quarks (qqq) or anti-quarks ($\overline{qqq}$) (called *Baryons*) or in quark-antiquark pair form ($q\overline{q}$) (called *Meson*).

  – **Baryons:**

    Baryons are hadrons which are made up of combination of three quarks or antiquarks. The Baryon number (B) (flavour quantum number) for baryons is +1. Behaviour of baryons is same as fermions having half integer spin. They have parity equal to one. We can have their anti particles called 'Anti baryon'. Examples of baryon are proton (uud) and neutron (udd) etc.

  – **Mesons:**

    Mesons are hadrons made up of combination of a quark and an anti quark. The Baryon number (B) for meson is zero. Behaviour of mesons is same as boson having integer spin. They have parity equal to -1. An anti meson do not exist. These particles have very short life time. Examples are $\pi^+(u\bar{d}), \pi^-(d\bar{u})$ and $\pi^0(u\bar{u}$ or $d\bar{d})$ e.t.c.

Fundamental Forces of Nature

There are four types of basic forces of nature which govern the interactions of matter i.e gravity, electromagnetic force, weak nuclear force and strong nuclear force.

Table 1.3: Fundamental forces of nature

Force	Strength	Range(m)	Mediator	Mass	Spin
Gravitational force	6×10^{-39}	infinite	graviton	0	2
Electromagnetic force	1/137	infinite	photon	0	1
Weak Nuclear Force	10^{-6}	10^{-18}	Weak Gauge Bosons	> 80 GeV	1
Strong Nuclear Force	1	10^{-15}	gluon	0	1

- **Gravitational Force**

  Gravitational force, the weakest force among other forces, has strength about 10^{-39} times of the strong force. We can easily observe that fact−If we rub a comb across our shirt to give it static electricity and then hold it over to some pieces of paper placed on a flat surface, we see that these pieces lift over the surface against gravitational force. So this force can be easily overcome just by mere charging.

  Along with it, range of gravity is infinite. The mediator of gravity is "graviton". It has not been observed experimentally because it is very difficult to find smallest domination of the weakest force. Graviton will likely be massless as proved by recent calculations. Its discovery will be the major discovery of the "String Theory".

- **Electromagnetic Force**

  The strength of electromagnetic force is less than strong force. Like gravity, it has infinite range but unlike gravity, electromagnetic force has both attractive and repulsive properties.

  This is the force responsible to keep atom together (i.e attraction between nucleus and electron). It is also responsible for keeping atomic sizes different (i.e heavy atoms have large number of electrons which repel each other and so atomic size is large).

The mediator of electromagnetic force is “photon”, a massless particle travels with the speed of light.

- **Weak Nuclear Force**

  It is operated in extremely short distances scale found in an atomic nucleus. The weak force is responsible for β decay.

  Its mediators are weak gauge bosons ($W^{\pm}$, Z) and are very massive.

  In this thesis, we will be dealing with weak nuclear force in detail and will be specifically discussing about Z boson.

- **Strong Nuclear Force**

  As the name suggests, its strength is highest and like the weak force, its range is limited to the subatomic distances. It is responsible for keeping quarks together into the proton and neutron and keeping proton and neutron inside nucleus.

  Its mediator is massless gluon as it ‘glues’ particles together.

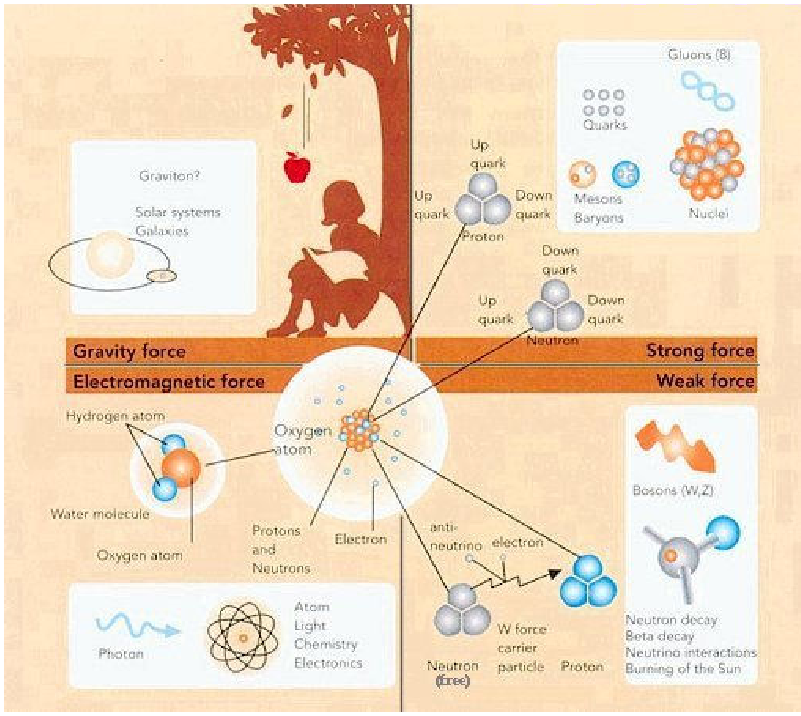

Figure 1.1: Fundamental forces of nature

Someone might think that why properties of all these forces drastically differ from each other? Why some mediators are heavy and other are massless? There should be a symmetry but we don't find it here...These are some open questions which need to be answer but scientists are not able to give a satisfactory answer of these questions at this point. All they understand is that it is necessary to consider such nature/properties of these forces. Only in this way, we can explain every phenomenon occurring in nature. So at present stage, we are only able to give answer of "HOW" still we are finding the reasons for "WHY".

The latter three interactions can be combined to a widely accepted model called 'Standard Model'.

1.2.2 Gauge Theories

When we try to look at our universe, we came to know that almost all naturally occurring things and phenomena have certain symmetry in them. So, the nature always creates beautification and order in everything. It is our strong desire to atleast try to approach to nature. For that purpose, man also tries to create symmetry in man made theories, devices and laws. It is our understanding that if we are able to introduce certain symmetry in a theory e.t.c, that would be a most natural (least ambiguous) theory. So it is necessary to introduce certain symmetry in Standard Model as well.

Gauge Theories, which are invariant under Lorentz Transformation, are special class of quantum theories. We describe particle and their interaction with the help of gauge theories. There are two kinds of particles in gauge theories; one of them are particles having charge (fermions and non abelian [4] gauge bosons) and others are particles which mediate interactions having gauge bosons (involving all abelian and non-abelian gauge bosons). Then non-abelian gauge bosons can interact with each other whereas abelian gauge bosons do not interact with each other.

We can describe three of the fundamental forces successfully in terms of gauge symmetry (having different dimensions unitary groups) up till now. We try to describe combinations of different gauge groups as $SU(3)_C \times SU(2)_L \times U(1)_Y$. In the group SU(N), the number of gauge boson is (N^2-1).

- **Quantum Chromodynamics:**
  The $SU(3)_C$ group describes the theory of strong interaction known as Quantumchromodynamics (QCD). The mediating particle of this theory are the massless "Gluons".

- **Quantum Electrodynamics:**
  The theory which describes electrodynamic interaction is known as Quantum

Electrodynamics (QED). By applying local gauge invariance principle to free Dirac Lagrangian, we can construct this theory. The operator $U = e^{iH}$ (where H is a real number) belongs to group (abelian) U$(1)_Y$. In order to construct invariant Lagrangian under local gauge transformation, we introduce A_μ, a vector field, necessary to achieve local gauge invariance. We can achieve desired symmetry only if A_μ is massless and long ranged. Resulting interaction Lagrangian for QED is

$$L_{QED} = (e\bar{\psi}\gamma^\mu\psi)A_\mu$$

where γ are Dirac matrices, e is electric charge and term in parenthesis describe the fermion current. Here Dirac field ψ quanta are fermions and electrodynamic field A_μ quanta are photons.

1.2.3 Cabbibo Kobayashi Maskawa Matrix

It was assumed until 1965 that when we change the signs of spatial coordinates (e.g x to -x, y to -y and z to -z) , the physics laws remain unchanged for a given system. When we invert certain coordinate, this mirroring effect is called Parity (P). It was later on observed by C.S.Wu that right handed neutrino, which is the mirror image of left handed neutrino, does not exist and so the symmetry of weak interaction is broken by parity operation. But to restore symmetry, we combine C (charge conjugation) operator with the Parity operator (where C operator converts particle into its anti particles). So, by applying a CP-operation to a left handed neutrino, we can convert it into a right handed anti-neutrino, that does exists.
Most of the phenomena occurring in our universe have the CP-symmetry or C and P symmetry separately. In particular, electromagnetic and strong interactions preserve these symmetries whereas weak interaction may violate C or P symmetry separately but CP symmetry is mostly preserved by weak interactions (but it is violated in certain rare cases).

The CP violation, arising in neutral K-meson system, can now be successfully interpreted in the standard model of electroweak interactions. It is closely related with the mixing matrix of quarks, the CKM matrix which connects the electroweak eigenstates (d, s, b) of d, s and b quark with their mass eigenstates (d', s', b') through following transformation (unitary).

$$\begin{pmatrix} |d'\rangle \\ |s'\rangle \\ |b'\rangle \end{pmatrix} = V_{CKM} \begin{pmatrix} |d\rangle \\ |s\rangle \\ |b\rangle \end{pmatrix} \tag{1.2.1}$$

where

$$V_{CKM} = \begin{pmatrix} V_{ud} & V_{us} & V_{ub} \\ V_{cd} & V_{cs} & V_{cb} \\ V_{td} & V_{ts} & V_{tb} \end{pmatrix}$$

CKM is unitary matrix by definition

$$\hat{V}^{\dagger}_{CKM}.\hat{V}_{CKM} = 1 = \hat{V}_{CKM}.\hat{V}^{\dagger}_{CKM}$$

CKM matrix unitary implies:

$$\sum_i V^*_{ij}.V_{ik} = \begin{cases} 0 & \text{if (j} \neq \text{k)} \\ 1 & \text{if (j = k)} \end{cases}$$

1.3 Lagrange Formulation

In Classical mechanics, we deal with a unique type of formalism called Lagrange formalism. We use Lagrange function L which illustrates the dynamics of a system. It is defined as

$$L = T(q_i, t) - U(q_i, \dot{q}_i, t)$$

where T is the kinetic energy and U is the potential energy of the system which are the function of generalized coordinates q_i and their derivatives $\dot{q}_i$. "Lagrange Density Function" $(\mathcal{L})$[5] is also important to introduce for relativistic field theories which is expressed as

$$L = \int \mathcal{L}(\phi_i, \partial_\mu \phi_i)\, \mathrm{d}^4x$$

where

$$\partial_\mu \phi_i = \frac{\partial \phi_i}{\partial x_\mu}$$

where we consider $\mathcal{L}$ as a function of complex field and their covariant derivatives.

The equation of motion for the system is obtained by using Euler-Lagrange equation which can be written as (by using calculus of variation)

$$\frac{\partial}{\partial x_\mu}\left(\frac{\partial \mathcal{L}}{\partial(\partial_\mu \phi_i)}\right) - \frac{\partial \mathcal{L}}{\partial \phi_i} = 0$$

- **Common Lagrange Densities**

  Lagrange density function for a spin one-half ($\frac{1}{2}$) free particle reads as

  $$\mathcal{L} = i\bar{\psi}\gamma^\mu \partial_\mu \psi - m\bar{\psi}\psi$$

  where ψ is "Dirac Spinor" and $\bar{\psi} = \psi^+\gamma^0$ and γ^μ is Dirac′s $\gamma - matrices$. In Lagrange density expression, first term denotes kinetic term and second term denotes mass term.

  Lagrange density function for a scalar particle having spin zero takes its form as (also called as Klein Gordon Equation)

  $$\mathcal{L} = \frac{1}{2}(\partial_\mu \phi)^2 - \frac{1}{2}m^2\bar{\phi}\phi$$

  For a massive spin 1 particle having vector field A, the Proca Lagrangian density function can be described by

  $$\mathcal{L} = -\frac{1}{4}F^{\mu\nu}F_{\mu\nu} + \frac{1}{2}m^2 A^\mu A_\mu \quad where \quad F^{\mu\nu} = \partial^\mu A^\nu - \partial^\nu A^\mu \tag{1.3.1}$$

1.4 Local Gauge Invariance

The laws of electro-magnetism remains invariant under unique transformations according to classical physics. The $\vec{E}$ and $\vec{B}$ fields are connected with the scalar potential (ϕ) and vector potential ($\vec{A}$) according to following relation

$$\vec{B} = \vec{\nabla} \times \vec{A} \quad and \quad \vec{E} = -\vec{\nabla}\phi - \frac{\partial \vec{A}}{\partial t}$$

Following transformation

$$A_\mu \rightarrow A'_\mu = A_\mu - \partial_\mu \Lambda(x) \quad with \quad A_\mu = (\phi, \vec{A}) \tag{1.4.1}$$

leaves the $\vec{E}$ and $\vec{B}$ field unchanged.(In above equation $\Lambda(x)$ is an arbitrary, differentiable scalar field). The above mentioned transformation is also applicable to quantum fields. So a local gauge transformation then reads

$$\psi(x) \rightarrow \psi'(x) = e^{i\alpha(x)}\psi(x)$$

but this transformation does not leave the Lagrangian invariant because of derivative term as

$$\begin{aligned}\partial_\mu \psi'(x) &= \partial_\mu \left(e^{i\alpha(x)}.\psi(x)\right) \\ &= \underbrace{e^{i\alpha(x)} i\psi(x)\partial_\mu \alpha(x)}_{\neq 0} + e^{i\alpha(x)}\partial_\mu \psi(x)\end{aligned}$$

So, if we want to achieve invariance under above transformation we replace partial derivative ∂_μ with the covariant derivative D_μ which is

$$\partial_\mu \rightarrow D_\mu = \partial_\mu + ieA_\mu \tag{1.4.2}$$

where $A_\mu(x)$ have to transform like this

$$A_\mu(x) \rightarrow A'_\mu(x) = A_\mu(x) + \frac{1}{e}\partial_\mu \alpha(x) \tag{1.4.3}$$

In this way, we can get the covariant derivative D_μ which retains same form as before after transformation. The Lagrangian density then becomes

$$\mathcal{L} = i\bar{\psi}\gamma^\mu \partial_\mu \psi - m\bar{\psi}\psi - e\bar{\psi}\gamma^\mu \psi A_\mu$$

which remains invariant under local gauge transformation. Here first two terms of Lagrangian describe the dynamics of free fermion and last term corresponds to coupling of electromagnetic vector field with the fermion.

In short, we can say that local invariant Lagrangian gives us a new vector function

A_μ which is same as the vector potential which we encounter in classical electromagnetism.

Furthermore, by looking at above Lagrangian we have to note that this vector field should be massless otherwise we will also have to consider a mass term

$$\frac{1}{2}m^2 A^\mu A_\mu$$

which can spoil the invariance under local transformation.
For getting Quantum Electrodynamics (QED) Lagrangian density, we add an additional term for spin-1 particles which represents dynamics of photons

$$\mathcal{L}_{\mathcal{QED}} = i\bar{\psi}\gamma^\mu\partial_\mu\psi - m\bar{\psi}\psi - j^\mu A_\mu - \frac{1}{4}F_{\mu\nu}F^{\mu\nu}$$

where $F^{\mu\nu}$ is defined in equation (1.3.1)

1.5 Theory of Weak Interaction

The weak interaction is responsible for transition between quarks and leptons. Experiments shows that left-handed leptons form doublets and right handed leptons form singlets (see Table 1.4). Here T represents the weak isospin. Fermions have weak isospin value equal to $\pm\frac{1}{2}$. A fermion can never decay into another fermion having same weak isospin value. For example up-type quarks (with $T_3 = +\frac{1}{2}$) will always decay into down-type quarks (with $T_3 = -\frac{1}{2}$). So a transition require particles having having weak isospin difference equal to ± 1.
Now we are going to describe another property called "Hypercharge" [6].

$$Y = 2(Q - T_3)$$

where Y is the hypercharge of the particle, Q is the electric charge and T_3 is the weak isospin third component. All left-handed antiparticles have weak isospin of zero whereas right-handed antiparticles have the opposite values of weak isospin.

Table 1.4: left-handed fermions

Generation 1		Generation 2		Generation 3	
Fermion symbol	T_3	Fermion symbol	T_3	Fermion symbol	T_3
e^-	-1/2	μ^-	-1/2	τ^-	-1/2
ν_e	+1/2	ν_μ	+1/2	ν_τ	+1/2
u	+1/2	c	+1/2	t	+1/2
d	-1/2	s	-1/2	b	-1/2

For left-handed and right-handed particles, invariant transformation under local phase is written as

$$\begin{aligned}\psi_L \to \psi'_L &= e^{i\alpha(x_\mu).\vec{T}+i\beta(x_\mu)Y}\psi_L \\ \psi_R \to \psi'_R &= e^{i\beta(x_\mu)Y}\psi_R\end{aligned}$$

with three generator $\vec{T} = (T_1, T_2, T_3)$ of SU(2) and Y for the U(1) transformation. For left handed particles, we introduce three vector fields $\vec{W}_\mu$ and for right-handed particles, we introduce one scalar field. For achieving local gauge invariance, the partial derivative then goes to covariant derivative as

$$\partial_\mu \to D_\mu = \partial_\mu - i\frac{g}{2}\vec{\sigma}.\vec{W}_\mu - i\frac{g'}{2}YB^0_\mu$$

Then resulting Lagrangian density becomes

$$\mathcal{L} = i\bar{\psi}\gamma^\mu\partial_\mu\psi - \frac{1}{4}\vec{W_{\mu\nu}}\vec{W^{\mu nu}} - \frac{1}{4}\vec{B_{\mu\nu}}\vec{B^{\mu\nu}} - g\bar{\psi}\gamma^\mu\vec{T}.\vec{W}_\mu\psi - \frac{g'}{2}\bar{\psi}\gamma^\mu B_\mu\psi_L$$

where $W^\pm$, Z^0 and A_μ are in linear combination of fields $\vec{W}_\mu$ and B^0 as

$$\begin{aligned}W^\pm &= \frac{1}{\sqrt{2}}(W^1 \mp iW^2) \\ Z^0 &= -\sin(\theta_W)B^0 + \cos(\theta_W)W^3 \\ A_\mu &= \cos(\theta_W)B^0 + \sin(\theta_W)W^3\end{aligned}$$

where θ_W is called the "Weinberg angle" which shows the fact that photon does not couple with the neutral neutrinos rather it can be coupled to the charge of the right handed and left-handed fermions. The Weinberg angle average is

$$\sin^2\theta_W = 0.232 \pm 0.000052$$

It is possible to write Lagrangian in terms of A, Z^0 and $W^\pm$ by introducing the concept of ladder operators $T^\pm = \frac{1}{2}(T_1 \pm T_2)$. Then in Lagrangian, in addition to the kinematic terms, we also include interaction terms for each gauge particle as given below:

$$\begin{aligned} A &: \sim e\bar{\psi}\gamma^\mu\psi A_\mu \\ W^\pm &: \sim g\bar{\psi}\gamma^\mu(1-\gamma^5)(T^+W_\mu^+ + T^-W_\mu^-)\psi \\ Z^0 &: \sim \frac{g}{\cos\theta_W}\bar{\psi}\gamma^\mu(c_v - c_a\gamma^5)\psi Z_\mu \end{aligned}$$

The photon gets coupled with leptons forming vector current having strength directly proportional to current. W and Z boson coupling shows vector and axial vector current. The term

$$\frac{1}{2}(1-\gamma^5)$$

operates onto the left handed Dirac particle and so Lagrangian couples W bosons to left-handed leptons. In case of Z boson, both currents contributes different strengths. A fermion having charge q_f can be coupled as

$$c_v = T_3 + 2q_f\sin^2\theta_W \quad and \quad c_a = T_3$$

Summarizing, Invariance under local gauge transformation leads us to the concept of unification of weak and electromagnetic interaction into a combined ($SU(2)_L \bigotimes U(1)_Y$) group. However, there is a contradiction between observed massive bosons and predicted massless boson since extra mass term can spoil gauge invariance.

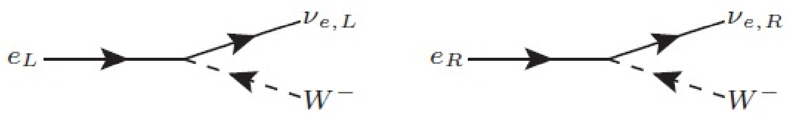

(a) observed (b) not observed

Figure 1.2: weak interaction is responsible for leptonic transitions. Weak current couples to left handed fermions and right handed anti fermions so right hand picture interaction cannot be observed.

1.6 Spontaneous Symmetry Breaking

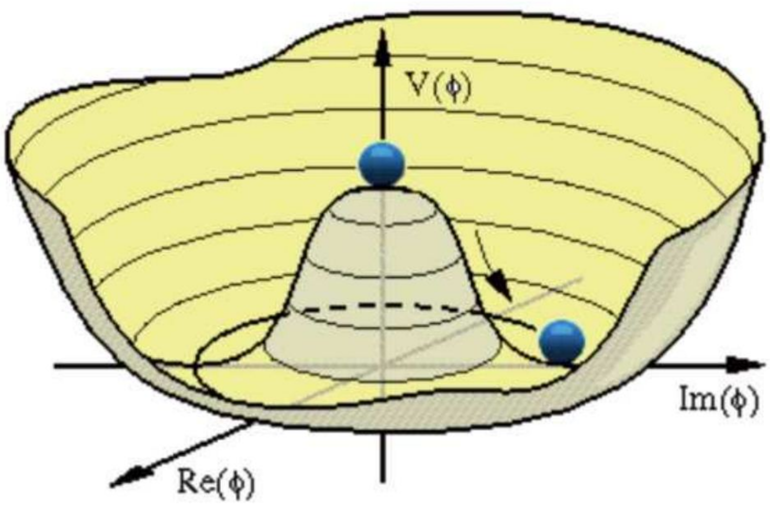

Figure 1.3: Illustration of symmetry breaking. At $\phi = 0$ we still see an unstable equilibrium. So any particle will prefer to reside into a state having much lower potential (ground state) with $\phi = \pm\nu$.

Brout, Higgs, Hagen, Englert, Guralnik and Kibble has proposed the idea of Spontaneous Symmetry Breaking for explaining the presence of masses of gauge bosons.

The concept of Spontaneous Symmetry Breaking is known to us from 'Ferromagnetism' in Solid State Physics. In absence of any external magnetic field, the energy of an atomic system is based on relative orientations of spins. If we rotate all spins it will not alter the system energy. But a ferromagnet undergoes a phase transition at critical temperature T_C and below this T_C, all spins will be pointing along one direction which causes symmetry of rotation less frequent about that axis so symmetry is broken spontaneously.

1.6.1 Global Symmetry Breaking

By adding a scalar field (complex), the "Higss Field", gauge bosons acquire masses. The complex field Lagrangian density, with self interacting field ϕ^4 and real valued fields $\phi_{1,2}$ reads as

$$\mathcal{L} = \underbrace{\partial_\mu \phi^* \partial^\mu \phi}_{E_{kin}} - \underbrace{(\mu^2 \phi^* \phi + \lambda(\phi^* \phi)^2)}_{E_{pot}} \tag{1.6.1}$$

$$\text{with } \phi = \tfrac{1}{\sqrt{2}}(\phi_1 + i\phi_2) \text{ and } \lambda > 0$$

Under global phase transformation, the above mentioned Lagrangian is invariant. For $\mu^2 \geq 0$, the potential V minimum is at $\phi = 0$. For $\mu^2 < 0$, all points are present on a circle which are given by

$$\phi_0 = e^{i\delta}\sqrt{\frac{-\mu^2}{\lambda}} \equiv \upsilon e^{i\delta} \tag{1.6.2}$$

which represents the potential minimum as shown in Figure 1.3. We can also rewrite ϕ as function of two scalar (real) fields χ_1 and χ_2 as

$$\phi = \frac{1}{\sqrt{2}}(\upsilon + \chi_1 + i\chi_2)$$

Expanding Lagrangian density around ground state, we get

$$\mathcal{L}' = \frac{1}{2}(\partial_\mu \chi_1)^2 + \frac{1}{2}(\partial_\mu \chi_2)^2 + \frac{1}{2}(2\mu^2)\chi_1^2 + const + O(\chi^3)$$

By looking at above Lagrangian, we can say that:

3^{rd} term having field χ^2 describes the massive particle having mass $m_{\chi_1} = \sqrt{-2\mu^2}$.

The field χ_2 describes the existence of a massless particle which shows transition from a ground state to another through δ as we can see in Eq.(1.6.2). The original radial symmetry is broken by the chosen ground state.

So the massless gauge bosons are the result of spontaneous symmetry breaking. There is no experimental proof of these gauge particles. We can avoid the emergence of these gauge bosons by coupling these to fields in 'Spontaneously Broken local Symmetry' which is described in next subsection.

1.6.2 Local Gauge Symmetry Breaking

The Lagrangian of Eq.(1.6.1) should be invariant under local phase transformation in order to achieve local gauge symmetry. So we need to introduce a substitute for derivative and a new gauge field A as given below:

$$\begin{aligned} \partial_\mu &\rightarrow \partial_\mu + iqA_\mu \\ A_\mu &\rightarrow A_\mu - \frac{1}{e}\partial_\mu\theta \end{aligned}$$

Again for simplicity, we prefer writing Lagrangian density in ground state

$$\begin{aligned} \mathcal{L} = \frac{1}{2}(\partial_\mu\chi_1)^2 + \frac{1}{2}(\partial_\mu\chi_2)^2 + \mu^2\chi_1^2 + \frac{1}{2}e^2\upsilon^2 A_\mu A^\mu \\ -e\upsilon A_\mu\partial^\mu\chi_2 - \frac{1}{4}F_{\mu\nu}F^{\mu\nu} - \mu^2\phi^*\phi - \lambda(\phi^*\phi)^2 \end{aligned}$$

In above Lagrangian, we can see a χ_1 field which represents a massive particle, field χ_2 representing a massless particle and a massive vector boson A_μ. Other than that, Lagrangian also have a term which couples vector field A_μ to Goldstone boson which is an non-physical phenomenon. As we observed a massive vector boson and as massless boson was not observed so it was supposed to be flaw. To overcome the problem, we have to write the complex field as

$$\phi \rightarrow \frac{1}{\sqrt{2}}(\upsilon + h(x_\mu))e^{i\zeta(x_\mu)/\upsilon}$$

For simplicity, we again define χ_1 and χ_2 in terms of h and ζ. So the Lagrangian density then changes as

$$\mathcal{L}'' = \frac{1}{2}(\partial_\mu h)^2 - \lambda v^2 h^2 + \frac{1}{2}e^2 v^2 A_\mu A^\mu - \lambda v h^3 - \frac{1}{4}\lambda h^4$$
$$+\frac{1}{2}e^2 A_\mu A^\mu h^2 + v e^2 A_\mu A^\mu h - \frac{1}{4}F_{\mu\nu}F^{\mu\nu}$$

Above Lagrangian represents a heavy scalar particle called Higgs boson "h" and a heavy vector boson "A" and couplings among them. In original massless Goldstone boson, the degrees of freedom are absorbed in heavy vector field having longitudinal polarisation as an extra degree of freedom.

1.6.3 SU(2)⊗U(1) Symmetry Breaking

To give a mass to $W^\pm$ and Z_0, we have to extend QED Lagrangian to by introducing a covariant derivative

$$\partial_\mu \to D_\mu = \partial_\mu \underbrace{-g\frac{\vec{\sigma}}{2}.\vec{W}_\mu - g'\frac{Y}{2}B_\mu}_{=(*)} \tag{1.6.3}$$

and also a complex doublet

$$\Phi = \begin{pmatrix} \phi^+ \\ \phi^0 \end{pmatrix} = \frac{1}{\sqrt{2}}\begin{pmatrix} \phi_1 + i\phi_2 \\ \phi_3 + i\phi_4 \end{pmatrix}$$

Because of theoretical constraints, the fourth scalar field is necessary. In ground state, the expectation value of $\Phi(x)$ is

$$\Phi = \frac{1}{\sqrt{2}}\begin{pmatrix} 0 \\ v \end{pmatrix} \quad with \quad v^2 = -\frac{\mu^2}{\lambda},\ \ \lambda > 0,\ \ \mu^2 < 0$$

In QED Lagrangian, the term $\mid (*)\Phi \mid^2$,then becomes

$$\mid (*)\Phi \mid^2 = \left(\frac{1}{2}v g\right)^2 W_\mu^+ W^{-\mu} + \frac{1}{8}v^2 \begin{pmatrix} W_\mu^3 \\ B_\mu^0 \end{pmatrix}^T \begin{pmatrix} g^2 & -gg' \\ -gg' & g'^2 \end{pmatrix} \begin{pmatrix} W^{3\mu} \\ B^{0\mu} \end{pmatrix}$$

where

$$W^{\pm} = \frac{1}{\sqrt{2}}(W^1 \mp iW^2)$$

In above equation, we can diagonalise second term so that gauge bosons appear.

$$\mid (*)\Phi \mid^2 = \frac{1}{2}M_W^2 W_\mu^+ W^{-\mu} + \frac{1}{2}M_Z^2 Z_\mu Z^\mu + \frac{1}{2}M_A^2 A_\mu A^\mu$$

with

$$\begin{aligned} M_A &= 0 \\ M_W &= \frac{1}{2}\upsilon g \\ M_Z &= \frac{1}{2}\upsilon\sqrt{g^2 + g'^2} \end{aligned}$$

The θ_W connects g and g' through

$$\tan\theta_W = \frac{g'}{g}$$

and the masses of W and Z bosons have relation as

$$\frac{m_W}{m_Z} = \cos\theta_W$$

Concluding, by using invariance under local gauge transformation SU(2)⊗U(1) and by introducing four scalar fields we result in a unified theory for electroweak interaction. In this model, photon is massless and weak gauge bosons acquire their masses. However, we can see a new massive scalar particle which is called Higgs boson. A new phenomena such as neutrino oscillations [7] shows that more extensions to Standard Model can not be avoided.

1.7 Z boson Theory

We now try to get familiarize ourselves with the Z boson theoretically in more detail.

1.7.1 Introduction

Z boson is the particle which mediates weak interaction. It is necessary to introduce such particle which is the cause of the occurrence of weak interaction. It was predicted very early for the true description of Standard Model.

Z boson is also very important for the explanation of the interaction of neutrinos among themselves [8]. Neutrinos can not interact via a photon because these are electrically neutral. So it was important to introduce Z boson there. As Z boson is very massive and it is very unstable so we can not observe Z bosons frequently. But it can be found in 'supernovae explosions' [9] and under conditions of early universe.

1.7.2 Properties

The major properties of Z boson are as follows:

- it is electrically neutral, charge = 0
- Z boson is its own anti-particle
- have half-life about 3×10^{-25} sec
- mass$\approx$91.1876$\pm$0.0021 GeV/c^2
- spin=1

As we have described earlier that Z boson is very unstable particle and it can not be observed easily so to know more about Z boson (its production and decays), we need to do a lot of effort for that purpose in the form of using accelerators. So, first we have to introduce ourselves with the Large Hadron Collider and Compact Muon Solenoid then we will be able to understand the Z boson experimental discovery and production e.t.c which is covered in next chapter in detail.

1.7.3 Drell-Yan Process

Drell-Yan process is a process in which hadron-hadron scattering takes place at high energies. In this process a quark from one hadron and anti-quark from another hadron collide, annihilate and produce a Z boson which decays into a lepton anti lepton pair.

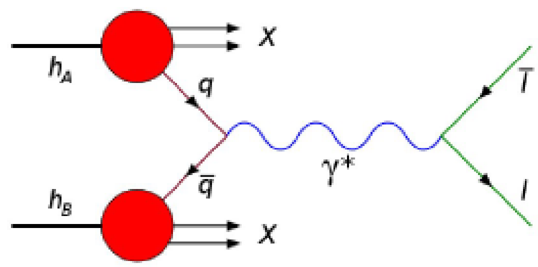

Figure 1.4: Drell-Yan Process

In 1970, 'Sidney Drell' and 'Tung-Mao Yan' first introduced this process which describes how to produce lepton and anti-lepton pair in colliders. Our interested channel is to study the Z boson decay to muon and anti-muon pair. So chapter 4 describes a detailed description of our research work.

Chapter 2

Experimental Overview

2.1 Large Hadron Collider

The Large Hadron Collider (LHC) is the world's most powerful and largest hadron collider situated at CERN near Geneva, Switzerland. LHC targets for new range of particle physics with 14 TeV center of mass energy and integrated luminosity of 10^{34} $\mathrm{cm}^{-2}\mathrm{s}^{-1}$.

Almost 10,000 scientists and engineers belonging different countries of the world, took part in building this huge collider. The circumference of LHC is 27 km and it is 574 feet beneath the Franco-Swiss border.

In 2012, we are able to achieve 8 TeV centre of mass energy of two colliding beams whereas it will go rise upto 14 TeV by the start of the year 2015 upon its reopening after two years halt due to maintenance work.

The data from LHC is analysed using a computer network (grid-based)[10] which connects 140 computing centres throughout the world. That grid is the largest computing grid of the world which connects 36 countries of the world.

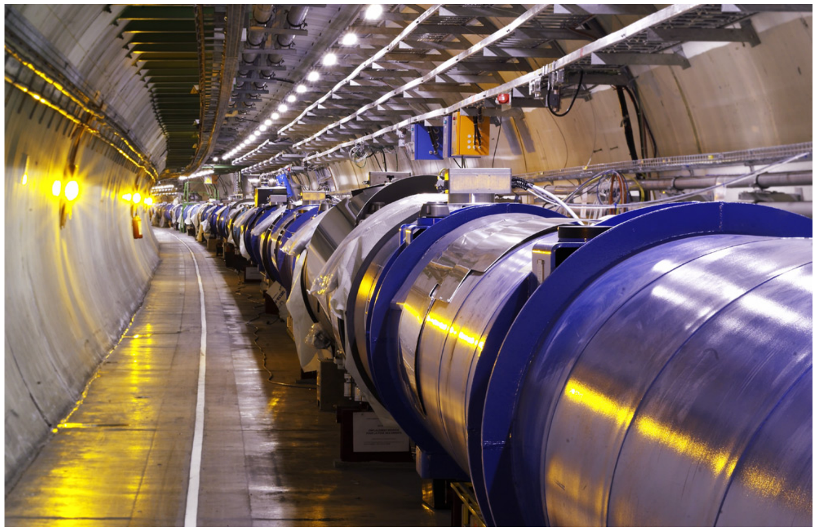

Figure 2.1: Large Hadron Collider

2.1.1 Goals of LHC

LHC is expected to answer some very important questions related to the early universe, its creation and the reason for masses of particles.

The main goal of LHC is to prove whether Standard Model is correct or not by searching Higgs Boson. On 4^{th} July 2012, CERN publically announced the discovery of a Higgs like boson which favours the Standard Model.

Other goals of LHC include the verification of the super-symmetry theory which is an extension of Standard Model. Also LHC is designed for detection of extra dimensions as predicted by "String Theory" [11]. Main goals also involve to look into the nature of "Dark Matter and Dark Energy" [12].

LHC is also expected to give some clues about "Grand Unified Theory" [13] which may be obtained by combining Electroweak Force with the Strong Force.

Scientists also hope to get reason for weakness of Gravitational Force. LHC is also finding reasons for asymmetry between matter and anti matter also it is searching for the nature of "Quark Gluon Plasma" which is thought to have existed in the time of early universe.

2.1.2 LHC Design

An underground tunnel (beneath Franco-Swiss border) was constructed between 1983 and 1988 whose breadth is 1.3 meters. This tunnel formally used for “Large Electron Positron Collider (LEP)”. Later on LHC was built by CERN from 1988 to 2008.

LHC contains two proton beams which make collision at four different points. Diople magnets deflect the beams in circular paths whereas many quadrupole magnets help the beams to be focused. Liquid helium is used in excessive amount to keep magnets at 1.9 K which is their operating temperature.

At 7 TeV beam energy, the velocity of the particles is about 0.999999991c but this much high speed can not be attained instantly but particles (protons) attain this speed gradually. So, first the particles are injected into “Linear Accelerators (LINAC)” which generates 50 MeV protons. These protons are then injected into “Proton Synchrotron Booster (PSB)” where these are accelerated to 1.4 GeV. After that, these are fed to “Proton Synchrotron (PS)” where their energy goes upto 26 GeV. In the end, protons are injected to “Super Proton Synchrotron (SPS)” from where proton achieve energy equal to 450 GeV. Then particles enter in big ring where these particles are accelerated to their desired beam energy 7 TeV.

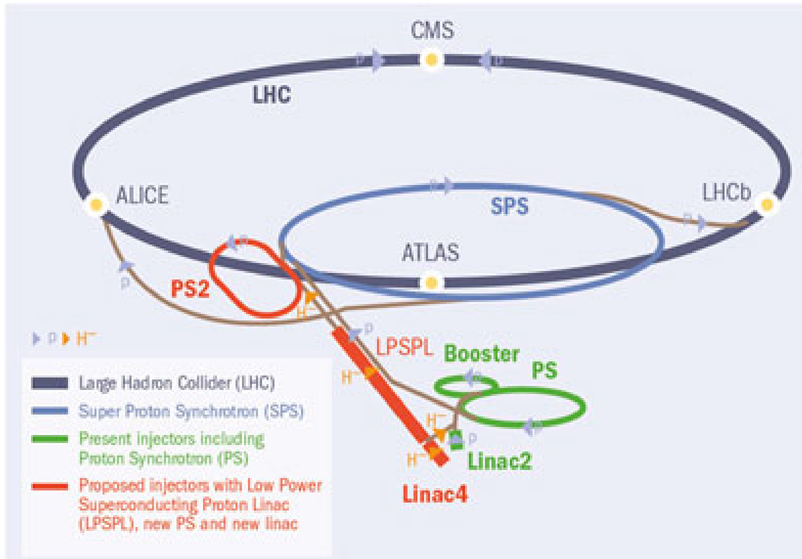

Figure 2.2: LHC Design

2.1.3 Detectors in LHC

There are six detectors which have been constructed in LHC. Here we present a brief overview of main detectors.

- CMS
- ATLAS
- ALICE
- LHCb
- TOTEM
- LHCf

Out of these detectors, four are main detectors whereas TOTEM[14] and LHCf are very small in size and are used for very specialized research fields.

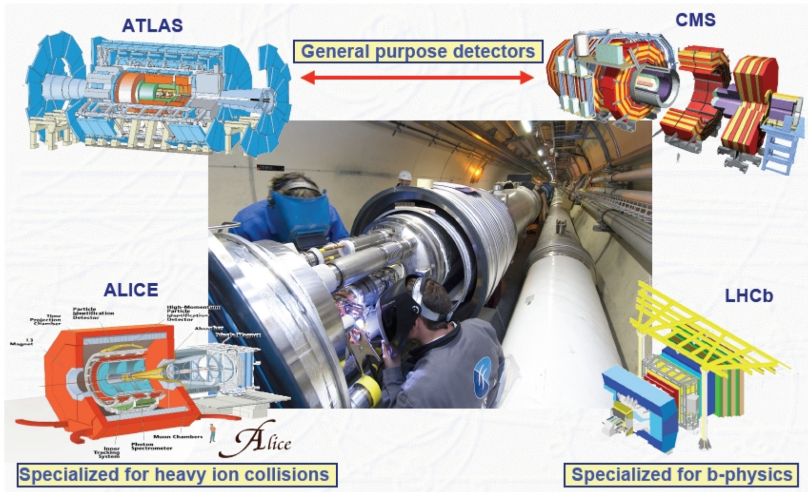

Figure 2.3: LHC and Detectors

- **CMS:**

  It is a general purpose detector whose main tasks are to look for Higgs Boson and to look into the mystery of dark matter. It is also used to answer some questions e.g How the universe is created? What is the thing which is giving mass to all particles of the universe? e.t.c.

- **ATLAS:**

  It is also a general purpose detector whose main task is to search for "New Physics" [15] and to look into extra dimensions [16]. It is also used to look for the extensions of standard model like "Super-symmetry" [17].

- **ALICE:**

  It is the detector which is specifically studying "Quark Gloun Plasma" [18] which remained for a short time after "Big Bang". ALICE is also specialized to study heavy ion collisions.

- **LHCb:**

  As the name suggests, LHCb is specialized to study b-physics. Also the purpose of this detector is to find some clues about the missing anti matter after the creation of earth and to look for reasons of asymmetry of matter and anti matter.

2.2 Hadron-Hadron Collision

At LHC, both colliding beams are of hadrons (protons). As protons are particles having small size so it is very difficult to get a head-on collision. To increase chances of collisions we have to squeeze and focus the beam as much as possible specially at the collision point 2.4.

According to an estimate, at the beam interaction point if we squeeze 100,000 million bunch of protons down to 64 microns (approximately equal to a human hair width), we can get only about 20 collisions per crossing. As the bunches cross each other after every 25 nsec so we can have around 600 million collisions per second. But still many protons may not have a collision at all and keep on circulating in beam ring time after time [19].

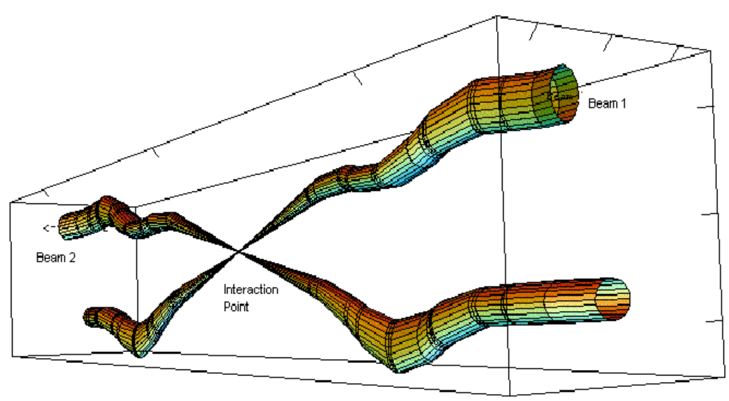

Figure 2.4: Relative beam size around lP1 (ATLAS) in collision

2.2.1 pp Total Inelastic Cross section

By definition

$$cross\ section = \frac{event\ rate}{luminosity}$$

The total proton proton cross section σ_{tot} can be defined as

$$\sigma_{tot} = \sigma_{elas} + \sigma_{diff} + \sigma_{inelas}$$

where σ_{elas}, σ_{diff} and σ_{inelas} correspond to elastic, diffractive and inelastic cross section respectively.
At 7 TeV center of mass energy, the total proton-proton cross section is about 110 mb. In which, the contribution from each part is

$$\sigma_{inelas} = 60\, mb$$

$$\sigma_{diff} = 12\, mb$$

$$\sigma_{elas} = 40\, mb$$

The elastic and diffractive cross section can not be seen by detector so only because of inelastic scattering the particles can be observed at high angles with respect to beam axis.

2.2.2 Event Rate

As

$$event\ rate = luminosity \times cross\ section$$

if

$$luminsity = 10^{34}\ cm^{-2} sec^{-1}$$

$$cross\ section = 60\ mb$$

Then inelastic event rate from previous example at nominal luminosity can be find out by

$$event\ rate = 10^{34} \times 60 \times 10^{-3} \times 10^{-24} = 600\, million\ events/sec$$

2.3 The LHC Beam and Luminosity Measurement

Large Electron Positron collider (LEP) was formally placed in same tunnel where now LHC is installed. The circumference of the tunnel is 27 km and the depth of tunnel below ground is 100 m. In LHC, both beams are of protons by keeping this point in mind that because of the high mass of proton, these particles suffer less from synchrotron radiations as compared to electrons. So, it is possible to achieve high centre of mass energy. As protons are packed into bunches so electromagnetic waves are used for acceleration of protons. To keep particles along circular path, 1232 dipole magnets are used. Also for focussing the beam, quadrupole and sextupole magnets are used.

As dipole magnetic strength is 8.33 T with the help of which energies of the beams go upto 7 TeV, we need to decrease the magnetic field strength which further decreases the dipole electric current. Superconducting magnet quench (collapse of superconducting state) can be avoided with the help of low current.

In 2008, because of loss of superconductivity and evaporation of liquid helium, many magnets were damaged heavily. During shutdown of machine in 2013, it will be possible to operate LHC with a justified risk at the designed luminosity.

The beam acceleration energies for the protons in different parts of the machine in listed in Table 2.1.

Table 2.1: LHC beam acceleration energies

Accelerators	Type	Beam Energy
Radio Frequency Quadrupole	linear	750 keV
Linear Accelerator 2	linear	50 MeV
Proton Synchrotron Booster	ring	1.4 GeV
Proton Synchrotron	ring	25 GeV
Super Proton Synchrotron	ring	450 GeV
Large Hadron Collider	ring	7 TeV

2.3.1 Measurement of Luminosity

Generally luminosity is defined as "measurement of brightness". The instantaneous luminosity is a quantity of experiment which depends on parameters of the beam. If σ is production cross section for a given process and N_{evt} are number of events then instantaneous luminosity can be defined as [20]

$$L = \frac{\dot{N}_{evt}}{\sigma} \quad where \quad \dot{N}_{evt} = \frac{\partial N_{evt}}{\partial t}$$

The integrated luminosity $\mathcal{L}$ is a term which gives us the amount of data which has been collected.

$$N_{evt} = \int L \,.\, \sigma \, \mathrm{d}t = \mathcal{L} \,.\, \sigma$$

To observe rare phenomena, it is essential to use high intense beams to get high integrated luminosity.

A plan for beam energy and luminosity in coming years has been prepared by CERN as follows:

- 2010−2011 is data taking period at 7 TeV energy. At the end of this period, the values for instantaneous and integrated luminosity are expected to be 1 fb^{-1} and 10^{32} $cm^{-2}s^{-1}$ respectively.

- A shutdown for 16 months period starting from early 2013 to increase energy and luminosity upto 14 TeV and 10^{33}cm^{-2}s^{-1} respectively.
- A second shutdown is possible in 2015, 2016 to increase luminosity upto 10^{34} cm^{-2}s^{-1}.
- One more shutdown is expected in 2020 to increase luminosity to $\approx 4{-}5\times10^{34}$ cm^{-2}s^{-1}.

2.3.2 Minimum Bias Events

Such collisions in which colliding protons are not smashed up or broken into pieces are called "diffractive" collisions and minimum bias events are those events in which non-single-diffractive (NSD) and inelastic events are considered. Also the events in which we select data with loose triggers to sample inelastic cross section in natural composition.

As the main source of bias in a detector is a trigger so we should take a high statistic sample which can minimize the trigger bias. But there will still remain inevitable biases because of energy resolution and imperfect detector's geometric acceptance. A trigger which selects all events which are not empty is called as a "perfect minimum bias trigger" [21].

2.3.3 Pileup Events

While taking a measurement with a CMS experiment, one has to suffer from "finite time resolution" of the sub detectors. In detector, it is difficult to differentiate between two collisions if these occur at nearly same time. Events obtained after overlapping energy deposits and interactions with detector material results into an event which is called as "pile up event". There is a difference between "true pileup" and "in-time pileup".

In-time pileup events refer to interactions from same bunch crossing. So, with the increase in number of protons per bunch, in-time pileup events increase. For actual amount of pileup, the number of reconstructed primary vertices is a very good measure for an event.

True pileup events refer to events from successive bunch crossings. So it is favoured by a small time gap between two consecutive bunches in a bunch train.

2.4 Compact Muon Solenoid (CMS) Detertor

As the name suggests, CMS detector is specially designed by installing calorimeters inside a solenoid. The total weight, length and diameter of the CMS detector is equal to 12,500 t , 21.5 m and 16 m respectively. The ATLAS detector, on the other hand, is large in size but light in weight. The weight, length and diameter of ATLAS detector is equal to 7,000 t, 46 m and 25 m respectively. At interaction point of two beams, the layout for both detectors is almost symmetric. The central barrel is flanked by "endcaps" on both sides. Inside magnet coil, calorimeter and tracking detectors are placed. Muon chambers are interleaved with the iron return yoke. Figure 2.5 gives a schematic view of CMS detector.

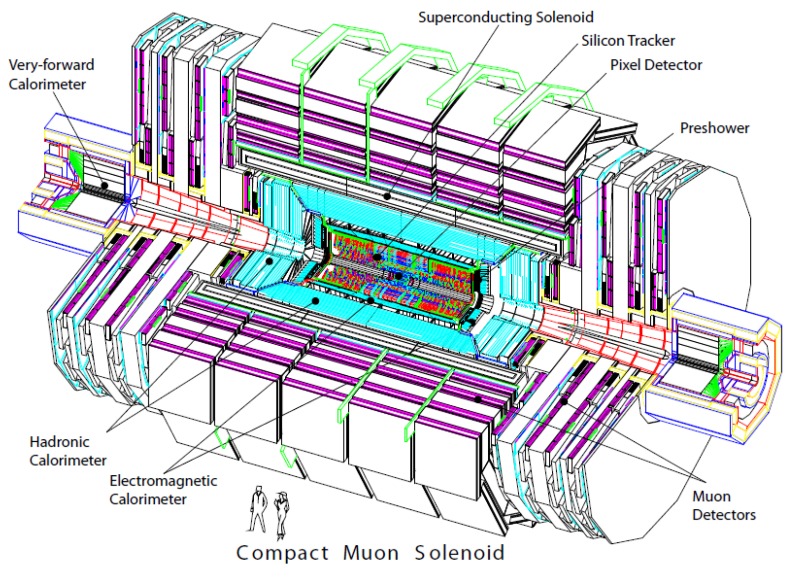

Figure 2.5: Schematic view of CMS detector and its components

2.4.1 Coordinate Conventions

The centre of CMS is assumed to be the origin of CMS coordinates system. Beam line in anti clockwise direction corresponds to z-axis. x and y are perpendicular axis in right handed coordinate system where y axis points upwards. The azimuthal angle ϕ is the angle in xy-plane (transverse plane) with respect to positive x-axis. The polar angle θ is measured with respect to positive z-axis.

Rapidity

In High Energy Physics, rapidity is defined as:

$$y = \frac{1}{2}\, ln \left(\frac{E + p_z}{E - p_z} \right)$$

Along beam axis, rapidity is an additive quantity for lorentz transformation. We choose rapidity because particle production is uniform in rapidity in hadron-hadron colliders. Also difference in rapidity is invariant under Lorentz boost.

Pseudorapidity

A similar quantity 'Pseudorapidity' is defined as

$$\eta = -ln\left(\tan\left(\frac{\theta}{2}\right)\right)$$

which depends only on polar angle θ. Pseuporapidity for a vector is zero if it is perpendicular to the beam axis and it goes upto infinity if vector goes along the beam axis. Note that in high energy limit ($E \approx |p|$) or for massless particles, pseudorapidity becomes equal to rapidity.

Transverse Momentum

Transverse momentum p_T for a particle is defined to be the momentum of the particle along the transverse plane (xy-plane). It is defined as

$$p_T = \sqrt{p_x^2 + p_y^2}$$

where p_x and p_y are momentum of particles along the x and y axis respectively.

2.4.2 CMS Detector Design

The CMS detector consists of following main parts.

- The Tracking System
- The Electromagnetic Calorimeter
- The Hadronic Calorimeter
- The Magnet System
- The Muon Chambers

A cross sectional view of the CMS detector having different layers for detection of different particles is shown in the Figure 2.6

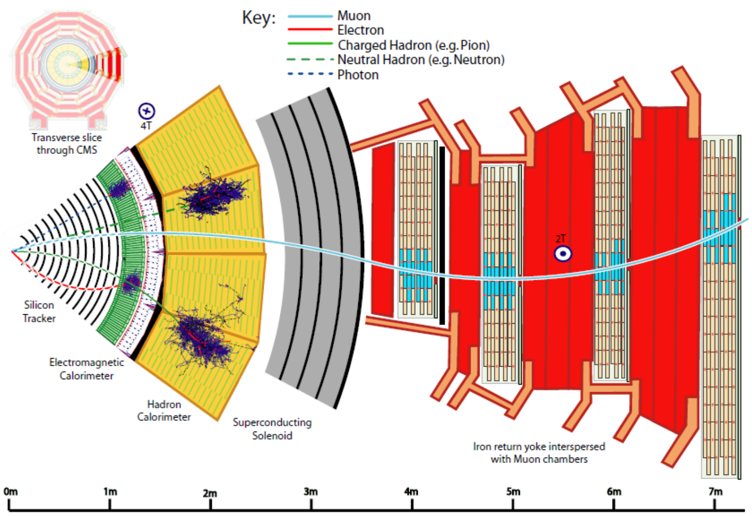

Figure 2.6: CMS view by layers

2.4.3 The Tracking System

The tracking system is the innermost sub detector system (see Figure 2.7). So, here the particle flux is maximum as it is next to interaction point of the beams. The construction of this system requires special attention towards spatial resolution and its component durability under hard interactions.

With the spatial resolution, we can differentiate between different charged particles. To achieve it, ‘Silicon Pixel Detectors’ having a size of 100×150 μm^2 each, are placed in three concentric layers. A spatial resolution of 10 μm and 20 μm can be achieved in $r\phi$-plane and z-direction respectively by using special filter techniques [22].

‘Silicon Strip Detectors’ are placed in 10 layers between (20−110) cm from intersection point of beams. Because of their shape, these detectors provide only 2D information about any hit. To get third dimension, these layers are twisted towards each others by 110 μrad. Depending upon distance to beam pipe, their single point resolution lies between (23−52) μm and (230−530) μm in $r\phi$-direction and z-axis respectively. Silicon strip detectors are much cheaper as compared to Silicon pixel detectors but in high particle flux, these detectors would show ambiguous results because of lack of third dimension.

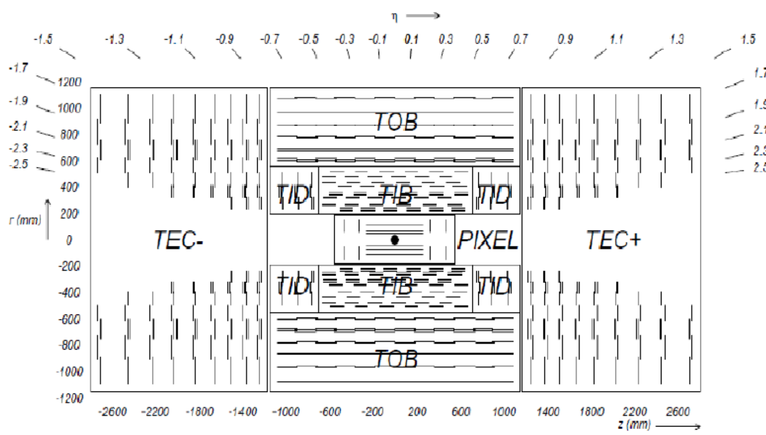

Figure 2.7: Schematic view of inner tracking system in rz-plane

All kinds of charged particles can be detected by the central tracking system. If a charged particle passes the silicon, the atoms of silicon get ionised which results in a measure of current because applied high voltage amplifies the ionization process. Magnetic field bends the charged particles. So in a detector, particles are located by the arc of a spiral. The curvature of the arc measures the momentum of the particle.

The tracking detectors allow us to measure accurately the secondary vertices position and the impact parameters [23]. Impact parameters are important to identify jets created by b-quarks (bottom quarks).

2.4.4 The Electromagnetic Calorimeter

The electromagnetic calorimeter (ECAL) (see Figure 2.8) made up of lead tungstate is a scintillation calorimeter. The incoming particles, electrons and photons, generate a cascade of secondary particles by electron positron pair production and bremsstrahlung [24] inside crystal. The number of generated photons is direct measure for energy of incident particle. Scintillation light in barrel region is detected by using silicon avalanche photodiodes because these can not sense the high magnetic fields. Vacuum phototriodes are used in endcap region as these can withstand high exposure of radiation in this region. Other than that, pre-shower detectors (made up of lead absorbers) and silicon detectors are used in front of endcaps to sort out photon pairs from π^0 decays and energetic single photons.

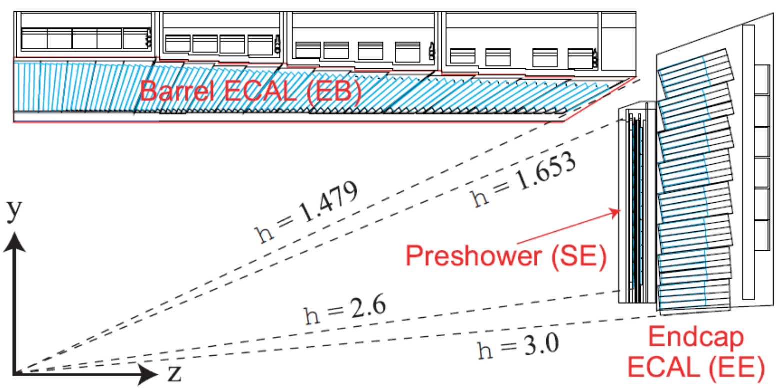

Figure 2.8: Schematic view of ECAL in rz-plane. Dashed line indicates pseudorapidity range which is not covered completely by ECAL.

In θ and ϕ direction, crystals cover 1^0 and these have length of 23 cm which leads to 25.8 radiation length of lead tungstate. For electrons having transverse energy equal to 75 GeV, ECAL has about 50% of the relative energy resolution.

2.4.5 The Hadronic Calorimeter

The Hadronic Calorimeter (HCAL) is basically a sampling calorimeter which made up of plastic scintillators and brass absorber material (see Figure 2.9). By inelastic process of scattering, hadrons generates a cascade of secondary particles. Major part of energy is deposited to the material which absorbs, only a little part of this energy is used for detection purpose in scintillator material. That is why HCAL has coarse energy resolution as compared to ECAL. Wavelength shifting fibres transport the scintillation light. Scintillation light clears fibres to hybrid photo diodes which can be operated at high magnetic fields. To increase accuracy of high energetic jets, additional detectors (outside magnetic coil) also support the calorimeter. Summing up, we can measure hadronic jets over a distance of 11 hadronic interaction length.

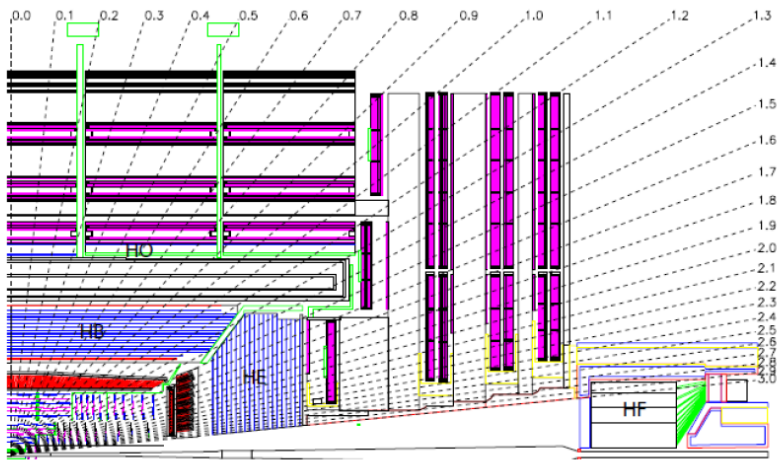

Figure 2.9: Schematic view of detector in rz-plane. HB and HO represents sub detectors of hadron calorimeter in inner and outer barrel region respectively. HE and HF represents endcap and forward region respectively. Dashed line represents pseudorapidity.

Forward calorimeter covers the pseudorapidity range ($3.0 < |\eta| < 5.0$) and it also monitors the instantaneous luminosity. As the above pseudorapidity range has high particle flux, so in this region, calorimeter is made up of steel absorbers having embedded quartz fibres.

The magical coverage of calorimeter allows a good measure of 'Missing Transverse Energy' E_T. But the response of ECAL and HCAL is different for particles (incoming) having same energy. Other than that, for whole pseudorapidity range, calorimeter is not uniform. So, we have to apply calibration for scale and off set of sub detector as function of transverse momentum and pseudorapidity. Details can be found in [25].

2.4.6 The Magnet System

The whole CMS experiment is built around a main device called 'The Magnet System'. The magnet of CMS detector is actually a 'Solenoid'. It consists of a 'Superconducting Coil' having length of 13 m and diameter of 5.9 m which is used to pass electricity without any resistance and it generates stronger magnetic field $\approx$ 4.0 T which is one million times stronger than that of earth′s magnetic field. This superconducting magnet system is the largest magnetic system of the world. It stores a large amount of energy as it can melt 18 tons gold.

The main purpose of this coil is to bend the incoming beam as very large amount of magnetic field is required to deflect such a highly energetic beam. The main parameters of the system are magnetic field having strength of 4 T, yoke having 14 m diameter across flats, axial yoke having length 21.6 m which includes endcaps and has $\approx$ 12,000 tons of total weight.

For $|\eta| < 1.5$, the magnet can accommodate the inner trackers and calorimeters so it is basically the 'supporting structure' for inner parts of the detector.

2.4.7 The Muon Chambers

The muons system is furnished with "iron return yoke" (see Figure 2.10). As muons are the minimum ionizing particles, so these can pass the iron whereas other particles can not traverse the iron. To cover large area range, gaseous detectors are used in muon chamber. In barrel region, aluminium drift tubes (DT) are used. In endcap, cathode strip chambers (CSC) are installed which can also work accurately in spatially varying B-fields. For getting precise value of muon momentum, DT and CSC provide spatial information.

Other than that, in barrel and endcap region, resistive plate chambers (RPC) are installed. For Level-1 trigger, RPCs provide fast information as these are able to operate at high rates.

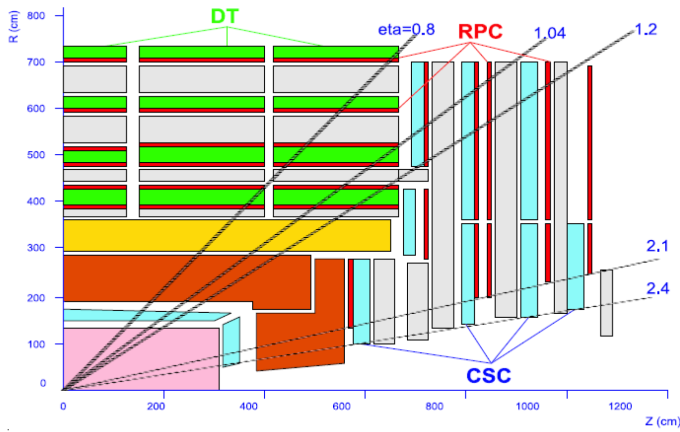

Figure 2.10: Schematic view of detector, highlighting muon chambers with DT, RPC and CSC. Iron return yoke components are shown in gray color, solenoid is in yellow.

In muon chambers, the detection efficiency for muons is greater than 98%. In barrel region, there is only some percent momentum resolution [26]. By using combination of inner tracking system and muon chambers, the path of muons can be precisely determined.

2.5 Trigger and Data Acquisition System

In CMS detector, every second around one billion collisions take place at designed luminosity but only a small part, around 400 events can be stored to disc which can be used for analysis purpose because of the limitation of computing facility. So we have to apply some triggers to reduce the size of the data which can be stored easily to machines. IT specialists are also trying to improve the computing facilities and we can observe a significance increase in the computing resources over the last months specifically during the shut-down of LHC machine after 2008 incident.

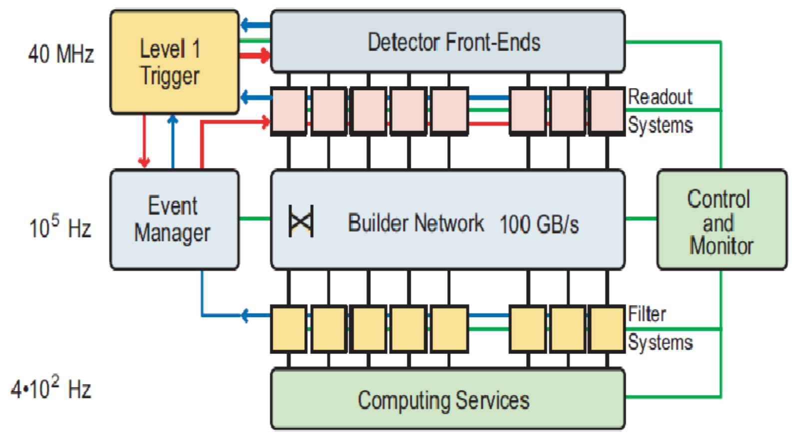

Figure 2.11: Data acquisition system of CMS experiment.

Level-1 trigger is implemented in hardware. The muon system and the calorimeter provide the information required to make trigger decisions. If a decision is made, hardware buffers store the full event data and if Level-1 trigger is failed, that data is flushed out. So the events which passes the first step can be forwarded to the second trigger step at rate of ≈100 kHz.

High Level Trigger (HLT) is implemented in software. So we can run algorithms which are identical or similar to offline reconstruction. HLT can also be reconfigured during its operation.

2.6 Z Boson at Hadron Colliders

In previous chapter, we got ourselves familiarize with Z boson theoretically e.g How Z bosons are theoretically predicted? What are main properties of Z boson? In this chapter, we will study some experimental facts about Z bosons e.g How Z bosons discovered experimentally? How we observe Z boson in LHC and CMS?

2.6.1 Experimental Discovery of Z boson

In 1983, Z boson was discovered at 'Super Proton Synchrotron' (SPS) in proton anti-proton collisions. Z boson was discovered in SPS by following channels:

$$Z \rightarrow e^{+} + e^{-} \;\; 4\, events$$

$$Z \rightarrow \mu^{+} + \mu^{-} \;\; 1\, event$$

The mass of Z obtained after fitting:

$$m_Z = (95.6 \pm 1.4)\, GeV$$

Discoverers were promptly awarded the Nobel Prize in 1984.

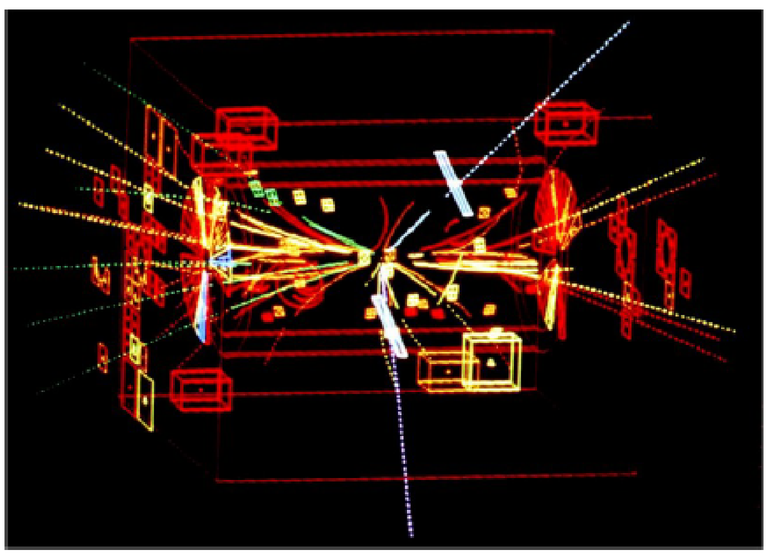

Figure 2.12: Discovery of Z in May 1983

Form 1989 to 2000, the study of Z boson was one of the major goals of 'Large Electron Positron Collider (LEP)'. Therefore it was named as Z−factory. In seven years of operation period, LEP produced around 7 millions Z particles.

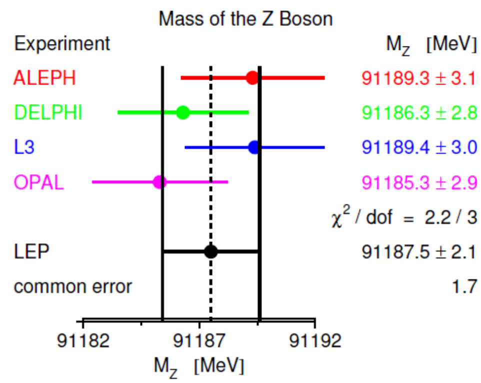

Figure 2.13: Results for measurement of Z mass at LEP. The overall results of four different experiments is shown in figure.

2.6.2 Production of Z Boson

At different colliders, Z bosons are produced by different methods.

- **At LEP**

  At LEP, colliding beams are of electron and positron are used so these particles annihilate which result into a mediating particle (Z boson) which further decays into a pair of fermion and anti-fermion. So by this mechanism, Z bosons are created at LEP.

- **At Tevatron**

  At Tevatron, colliding beams are of proton and anti-proton so quark from proton beam and anti-quark from anti-proton beam annihilate and create a Z boson which further decays into a pair of lepton and anti-lepton.

(a) (b)

Figure 2.14: Z production (a) at LEP (b) at Tevatron

- **AT LHC**
  At LHC, proton proton beams are used. The quarks present in protons interact through gluon exchange so they can split into $q\bar{q}$ pair which produces a 'sea of particles'. With the increasing energy of beams, sea of particle increases which further decays to W and Z. Mainly Z bosons are generated by annihilation of $u\bar{u}$ and $d\bar{d}$.

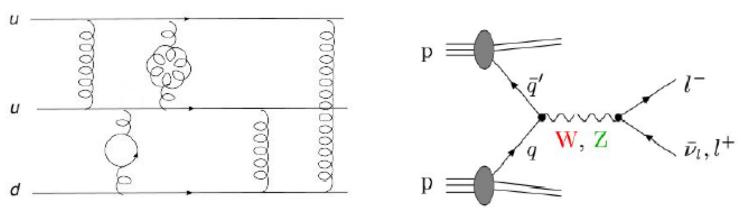

(a) (b)

Figure 2.15: (a) quark interaction via gluon (b) Z production at LHC

2.6.3 Decay of Z Boson

As Z boson is a neutral particle so the sum of charge of its daughter particles should be zero. So it decays to a particle anti-particle pair. Applying conservation laws, the Z can decays through following channels or decay modes.

- 10% of the Z bosons decay into a pair of lepton and anti-lepton. As there are three lepton families which exist in nature, so among leptons, Z can decay into

$\mu^+\mu^-$, e^+e^- and $\tau^+\tau^-$. The decay probability for each pair is equal which is also termed as 'Branching Ratio'.

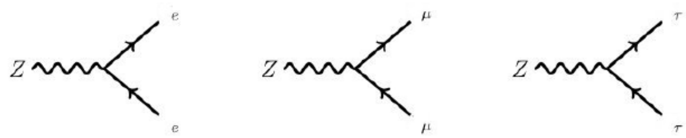

Figure 2.16: Z decay into lepton anti-lepton

- 20% of the Z boson decay to neutrino anti-neutrino pair. As neutrino are considered to be massless, travel with speed of light and never interact with anything as has no charge so we can not detect a neutrino in a detector but can be inferred through missing transverse energy. Among neutrinos, Z can decay into following modes.

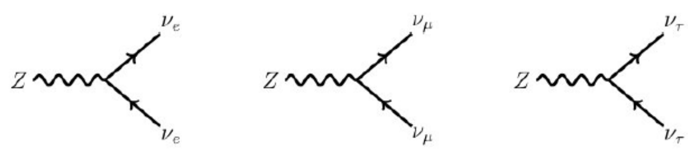

Figure 2.17: Z decay into neutrino anti-neutrino

- 70% of the Z bosons decay to a pair of quark anti-quark. These pairs form particle showers called as "Jets" in detector. Since six flavours of quarks exist, each having three colors, so there are 18 decay modes which are possible for Z decay into quarks.

So, in total there are 24 possibilities for Z decay. Excluding its decay to neutrinos (which are not visible), we can observe its 21 decay possibilities, among which the decay channels which can be detected easily are Z decay to electron positron and muon anti-muon.

Chapter 3

Software Tools and CMSSW Framework

3.1 Event Generation

For a physical process, the Monte Carlo event generation is basically based on probabilistic results of the mathematical description of that specific process. The cross section of an event describes the probability for occurrence of that event. The cross section for a hadron hadron collision is obtained be convolution of the parton distribution function with the partonic cross section $d\sigma_{ij \to l_1 l_2}$. For a $2 \to 2$ process, cross section is defined as:

$$d\sigma = \sum_{ij} \int dx_1 dx_2 f_i(x_1, Q^2) f_j(x_2, Q^2) d\sigma_{ij \to l_1 l_2}(x_1, x_2)$$

where $\sum_{ij}$ gives us the sum over all partons and f_i is the probability of ith parton having fraction of longitudinal momentum x at scale of Q^2. In any collision, for hard interaction (initial interaction for between partons), momentum transfer Q^2 is large. So, by using perturbation theory, we can find out partonic cross section. However, for a full event, it is not possible to do such calculation.

CMS collaborates with a number of generators. Some of these are PYTHIA [27], HERWIG [28], MADGRAPH [29], POWHEG [30]. Last two focus on calculating matrix elements. Parton QCD evolution is also included in PYTHIA and HERWIG.

3.1.1 PYTHIA

Pythia, written in FORTRAN 77 language, is a general purpose Monte Carlo event generator for lepton and hadron collision processes. Since 1978, it is widely used in high energy physics for event generation purpose. Pythia 8 is written in C++ completely. But major officially produced events are based on Pythia 6.4.

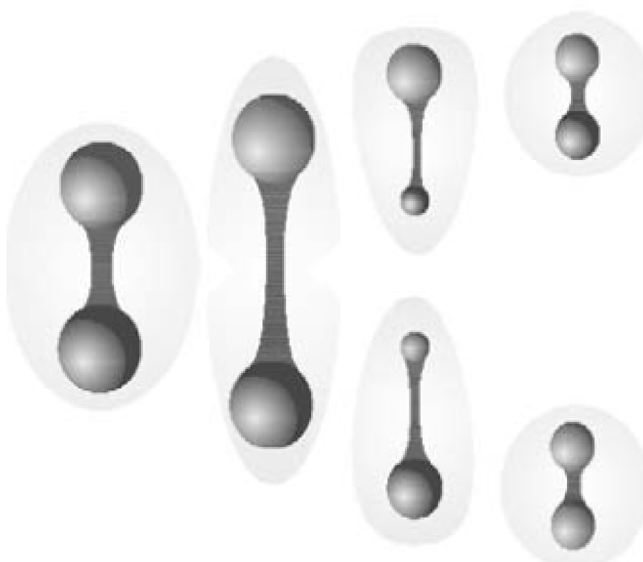

Figure 3.1: Coloured objects cannot exist isolated. When separated, the field forms gluon strings. At a distance of about $1fm$ the string fragments and produces pairs of $q\bar{q}$.

As an input for Pythia, two particles with some centre of mass energy are used. In Pythia, we deal with many $2 \rightarrow 2$ and some $2 \rightarrow 3$ processes as hard processes.

In Pythia, without any time taking calculations of higher order matrix element, one parton may be divided into several partons. According to Lund String Model, when the distance between color particles becomes larger than 1 fm, a virtual string breaks and new $q\bar{q}$ pairs are formed (see Figure 3.1).

Pythia allows use of other generators e.g POWHEG for hard sub processes e.g $q\bar{q} \to Z + jets$. These packages include precise calculations for Feynman diagrams and it include angular distributions and interference terms.

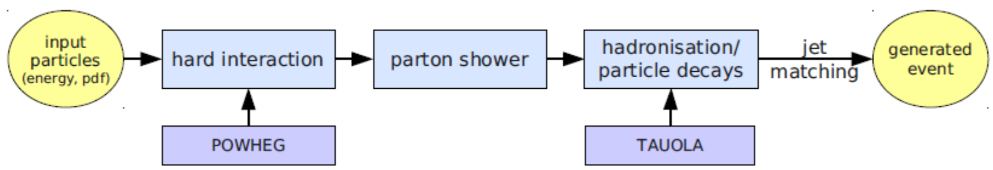

Figure 3.2: Workflow of Pythia

Figure 3.2 describes Pythia workflow. In first step, hard process is initiated for some input particles, we can also involve external libraries e.g POWHEG. With the help of parton shower method, coloured particles can be processed. Decay of particles can be described by using external libraries e.g TAUOLA. Some processes involve jet matching algorithms (to avoid double counting of jets). We can do it by using CMSSW.

In CMS experiment, we frequently use Pythia for event generations as it is fully integrated into CMSSW. So, we can directly control it with configuration files rather than using FORTRAN commands. We can directly call Pythia functions under user modules inside CMSSW. We can directly store events in standard form (e.g HEPMC) so that it can be used further if needed.

3.1.2 Matrix Elements at NLO Precision

Pythia provides results of matrix elements at leading order precision. In case of W and Z bosons, it is necessary to have precise calculations at next to leading order precision (NLO). But without any modification, using NLO matrix element with parton Pythia shower, may lead to wrong results as shower algorithm includes approximations for next to leading order effects.

It can be corrected by subtracting approximated corrections. A "statistical weight" is assigned to each event which shows the calculated correction. But a side effect is that the events can also be assigned as negative weight.

3.2 ROOT

ROOT [31] is an object oriented framework which is used widely in high energy physics community for analysing large scale data. ROOT, written in C++ language, is much simple to use than its predecessor PAW which was written in FORTRAN language. ROOT may be used interactively or by using some user interface.

ROOT can also create histograms which can be fit to different functions. Also it provides classes for data input/output operations and stores tuples of user defined classes and values. We can also reduce our file sizes which takes less time in data processing. ROOT can even handle very large amount of data easily.

3.3 CMSSW Framework

CMS collaboration has provided a framework with the help of which we can perform analysis study for an experiment, that is called as CMS software (CMSSW). It includes generation, simulation and processing of data for an experiment.

CMSSW very easily executes different tasks and we can also perform comparison studies as we can change any parameter according to our will very easily. Also it provides many examples and tutorials with the help of which less experienced users and get advantage in writing their own program.

3.3.1 Modular Architecture

With the help of CMSSW, it is possible to process data having different modules, each having specific task. The user has to run configuration file for the process under CMSSW framework. Framework loads all libraries and modules which are necessary, in response.

At the starting of each job, source module provides the necessary actions for an event to be selected. These events can be generated by using MC generator or can be read from a file.

The event data is further passed through all modules step by step. There are three different classes for these modules.

- **Filter Module**
  The job of filter module is to select or reject the events after matching the selection criteria. For example if we are interested in selecting two muons then the events with less than or greater than two muons will be rejected by filter module.

- **Producer Module**
  With the help of producer module, we can add new objects to event. User can write his own module with the help of some existing information. Objects which are added to an event may be transient which means these can only be processed but not written to disk.

- **Analyzer Module**
  Analyzer modules can be used for studies. The job of these modules is to store and generate parametric quantities in form of graphs and histograms.

It is also useful to store our data in a condensed form called *ntuples*. The size of this data is much smaller so it can be processed in short time.

3.3.2 Detector Simulation

Using CMSSW framework, it is possible to generate such events having particles traversing through CMS detector, keeping in view all of the detector effects. CMSSW includes GEANT 4 [32] package that can simulate the particle interaction with detector matter very precisely. GEANT 4 package is created by collaboration of scientists from high energy and medicine. This package includes all effects and processes e.g Compton Scattering, Rayleigh Scattering and Bremsstrahlung e.t.c.

We can also find out position and strength of interaction of particle with detector material. For example we can count hits in detector. This step is called as "Digitisation" which deals with the intrinsic detection threshold and modelling of electronic noise. This step gives us identical output as one can get using CMS detector.

By using CMSSW framework, we can easily modify detector components and performance. Systematic detector effects can be simplified by this modularity.

3.3.3 Fast Simulation

In this simulation, particle interaction with material is not calculated in detail. Rather particle path in detector is smeared which can be compared directly with real data or full simulation. It is called "FastSim" as this simulation just need to look to tables and so it does its job in a fraction of time that full simulation takes.

3.3.4 Event Data Model

Event data model is the integral part of CMSSW. It is basically a container for objects for example raw data, different parameters or any derived quantity. We can add new objects to events. We can store these events in the form of ROOT files so we can access these files using "Framework Lite (FELITE) libraries.

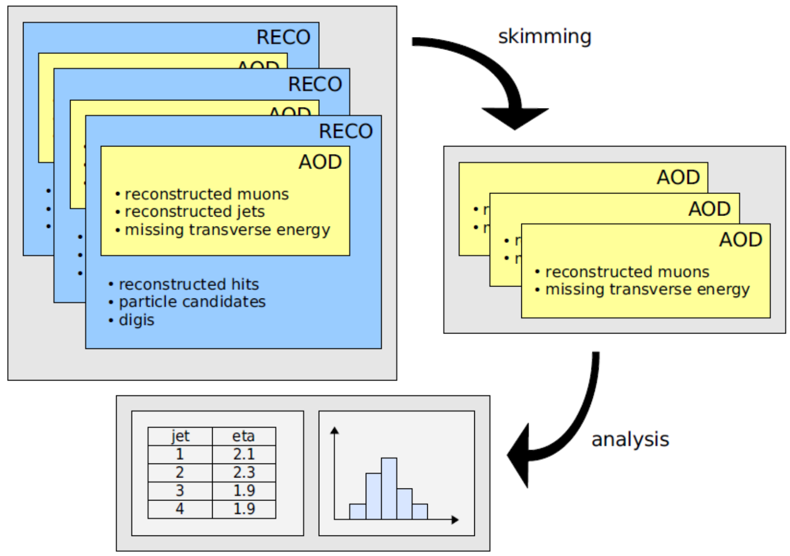

Figure 3.3: Typical analysis model for Pythia

The EDM allows refining (Skimming) of data in which reduction in the size of data occurs which further reduces processing/runtime of analysis and it also saves storage space. CMSSW includes some pre defined data tiers e.g RECO in which all reconstructed objects are included and AOD (Analysis Object Data) which includes objects needed for specific physics analysis.

3.4 LHC Computing Grid

While performing a CMS experiment, we have to deal with a large amount of data produced by MC studies or by CMS experiment itself. As we need this data again and again for analysis studies so all of this data should be stored somewhere in an organised manner.

The goal of CMS computing model is to provide access to this data without interruption to all scientists throughout the world attached with the experiment. The

HEP community has selected a model which has distributed its resources geographically and can be accessed via common interfaces. We call this distributed computing as "Grid Computing". This computing grid distributes the workload among all connected computing resources. So Worldwide LHC computing grid is made by all sites participating in LHC experiment.

3.4.1 WLCG Structure

The grid computing model is organized in four tiers. Tier-0 receives data directly from experiment. It runs event reconstruction and archives data on tape storage. Raw data and reconstructed data then moved to Tier-1 site. In Tier-1, data can be used for reconstruction, skimming and other tasks. Along with it, Tier-1 also transfers data to Tier-2 sites. Tier-2 contributes to processor intensive task e.g production of Monte Carlo and provide computing resources to users. Tier-2 are fully embedded to official CMS computing tasks. Tier-3 sites are smallest unit and provide resources to local groups. For interactive analysis and production of private MC, these are suitable.

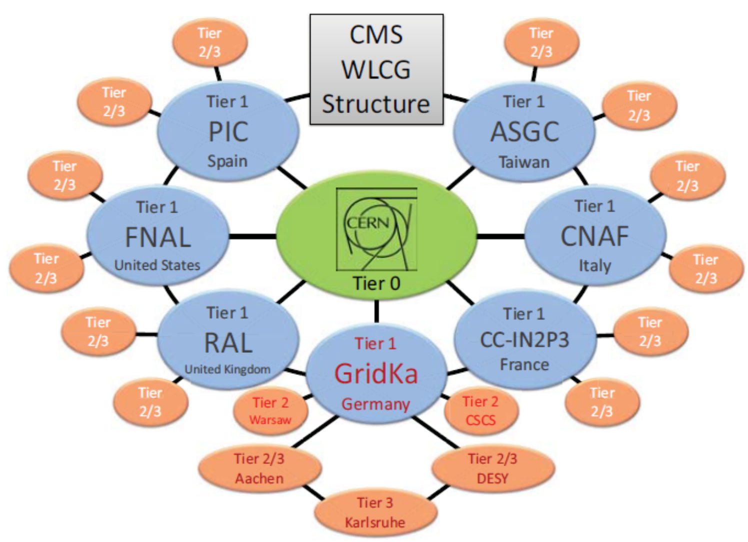

Figure 3.4: WLCG Tiered structure

3.4.2 Grid Services

Grid system provides access to all data and computing resources through standard services in simple way. Within grid, to access rights for resources, users need to have a membership in "Virtual Organization (VO)". This authentication is based on having personal grid certificates. A VOMS service can provide us a temporary certificate, called grid proxy, which is identity of user to grid services.

3.4.3 Site Services

Storage element (SE) is a connection between grid and local mass storage system. Storage elements keep all data to hard disk and it also does the job of translating grid commands into a language of storage system.

With the help of User Interface (UI), local user can have access to grid services. They can easily submit and monitor their jobs on grid and can also transfer data files to SE.

3.5 National Centre for Physics

National Centre for Physics (NCP), established in 1999, is a research institute for physics and allied disciplines in Pakistan. NCP establishment was the dream of Dr. Abdul Salam. The main purpose of this institute is to provide proper experimental and theoretical facilities to scientist associated with it and to bring Pakistani researchers close to International Scientific Community.

3.5.1 Collaboration with CERN

In field of Experimental High Energy Physics, NCP [33] is in collaboration with CERN. NCP has prepared, tested and assembled "Resistive Plate Chamber" (RPC) used in CMS muon system at LHC. RPCs have very high time resolution about $1-2$

nanoseconds and these are gaseous detectors which can be made by two parallel plates of Bakelite.

Along with it, different scientists and research students of Pakistan are doing Physics Analysis Study of different channels using LHC data. They are using NCP computing resources for copying and analysing data for their physics analysis.

3.5.2 NCP Computing Resources

In order to analyse very large amount of data coming from LHC, it is necessary to have advance scientific computing resources. For managing and accessing LHC data, concept of computing grid is used. NCP is partner of CERN in Worldwide LHC Computing Grid project and LHC Computing Grid (LCG) is the only node available to Pakistan.

3.5.3 LCG Node

LCG node is maintained and deployed by computing group at NCP. Effort was started in October, 2003 in a workshop named as "Grid Technology Workshop". During tutorial, 30 machines were used to enable users to communicate them with the deployed test-bed.

NCP is now a testified and certified grid node in Pakistan. It is certified by CERN and added to (GOC) Grid Operation Centre website. NCP is first in Asia, fifth in South Asia having certified grid node.

3.5.4 PK-Grid-CA

The Pakistan Grid Certification Authority [34] is responsible of issuance of grid certificates. These digital certificates (issued by trusted Certification Authority) are required for being fully operational grid node.

The efforts for this certification authority were started in 2003. From September 2004, PK-Grid-CA started its operation. Now NCP can issue host and user certificates to all grid partners. It is certified by (EUGridPMA) European Grid Policy Management Authority.

Chapter 4

Measurement of Z boson Production Cross Section using Muon Pair

Z boson has been a major subject of study for various experiments since its discovery. The study of properties and production of Z boson is not only a test of standard model but also its study is very important for parton density functions for hadron colliders and it is even sensitive to many exotic physics models. Because of the large production cross section of Z boson ($\approx 1.12 \pm 0.01$ (stat.)± 0.02 (syst.)± 0.06 (lumi.) nb) [43], it is used for calibration of CMS detector. Its study is also important for many other processes e.g Higgs searches, resonances and New Physics. Compact muon solenoid detector design makes it very suitable for detection and reconstruction of muons which leads to measure Z boson decay to muons.

In this chapter, analysis study which is particularly dedicated to $Z \to \mu^+\mu^-$ channel is introduced which leads to measure Z boson production cross section using 2012 dataset.

4.1 Event Topology

Z boson decay to two muons is a process having specific final state. Two muons finally detected by the detector have transverse momentum on the average of 45 GeV/c so that they can reconstruct a Z boson as their parent particle which should be nearly at rest. CMS detector shows good momentum resolution in the specific region of phase space for reconstructed muons. As created by electroweak process, these muons are not involved in any additional activity in general.

4.2 Event Generation

Generator level study of any analysis is the study without including detector effects. On the other hand, it is a quick way of understanding the sensitivity of a particular study.

In this analysis, first generator level study was done by using “Stand alone Pythia” and then by using “CMSSW Generator Level” just to cross check. Results and distributions were found consistent.

4.2.1 Stand Alone Pythia

To generate events for $Z \to \mu^+\mu^-$ by using stand alone pythia, some cuts and processes were initiated (see Table 4.1).

Table 4.1: Pythia stand alone cuts and processes

process	WeakSingleBoson:ffbar2gmZ(GeV/c^2)
hard process cuts	PhaseSpace:mHatMin = 50.
	PhaseSpace:mHatMax = 130.

Due to a low mass peak in Figure 4.2 (a) and 4.3 (a), the cuts mentioned in Table 4.1 were necessary to apply to reduce the contribution due to virtual photon.

4.2.2 CMSSW Generator Level Study

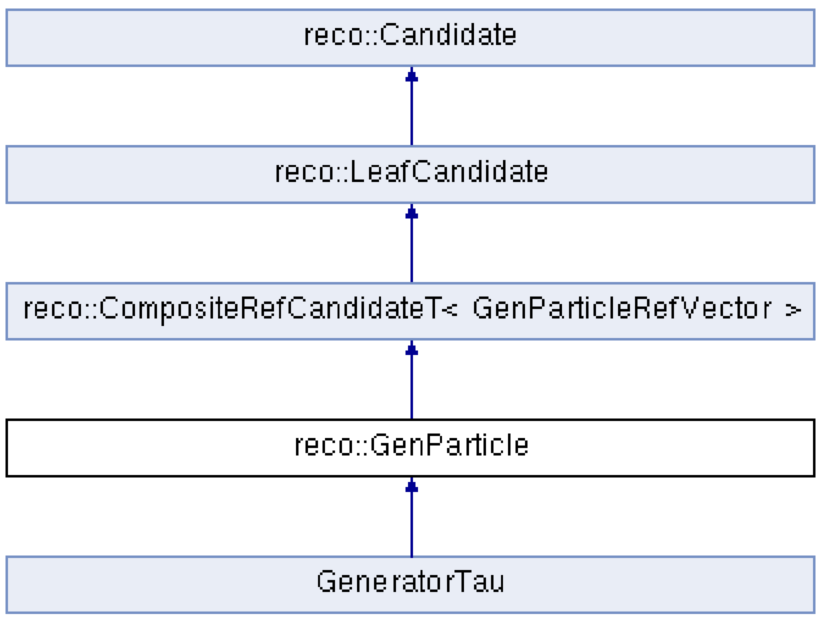

Figure 4.1: Inheritance diagram for reco::GenParticle

For CMSSW generator level study, reco::GenParticle class was included in analyser code which is a class inherited from reco::Candidate (see Figure 4.1) and plots for different kinematic variables of muons and Z boson were obtained.

For CMSSW generator level study, MC dataset in Table 4.1 was used. In the dataset name, M-20 GeV/c^2 refers to a lower mass cut on Z boson mass (the value is much smaller then the cut in Table 4.1 for Pythia standalone) so a low peak was observed in muon p_T and Z mass distribution because of virtual photon contribution.

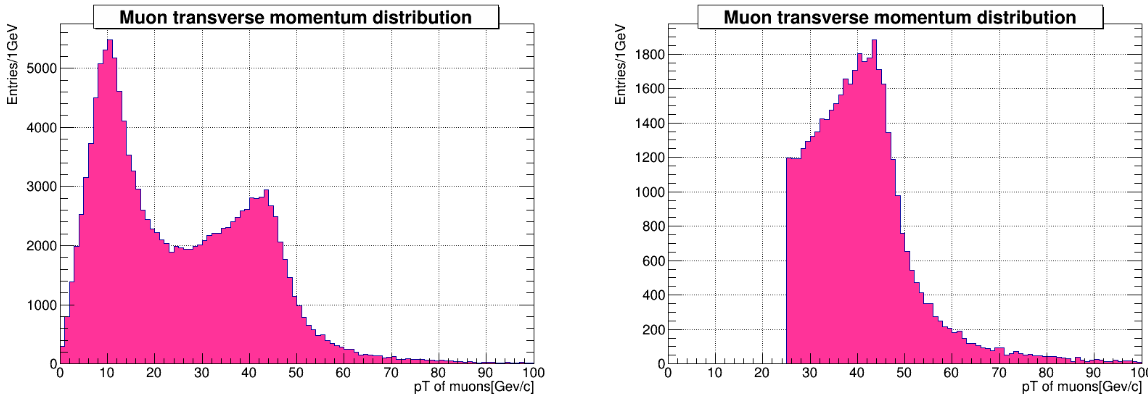

(a) (b)

Figure 4.2: (a) Generator level distribution of muon transverse momentum without using any cut on muon p_T. (b) Generator level distribution of muon transverse momentum after using cut on muon p_T.

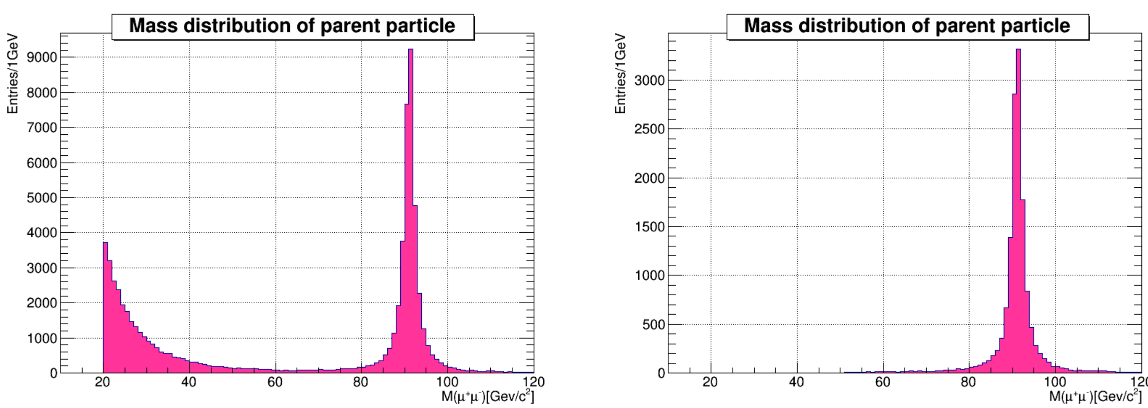

(a) (b)

Figure 4.3: (a) Mass distribution of reconstructed parent particle without using any cut (b) Mass distribution of reconstructed parent particle after using muon p_T cut.

- **Discussion of Plots:**

  MC dataset had a lower mass cut on hard process (i.e $M_Z > 20$ GeV/c^2) which could be easily verified by looking at mass distribution of the parent particle. A lower mass peak was observed in both plots which was an ambiguous case of resonance decays as mentioned in pythia documentation. According to that photon when participate in shower evolution can be assigned with heavy mass particle so it can be doubly counted. To avoid the situation (off-shell photon in shower evolution), a lower mass cut on the hard process or on muon momentum should be applied so after applying cuts on muons (e.g $p_T > 25$ GeV/c & $|\eta| < 2.1$), the plots were modified and the lower peak vanished (see 4.2 (b), 4.3 (b)) .

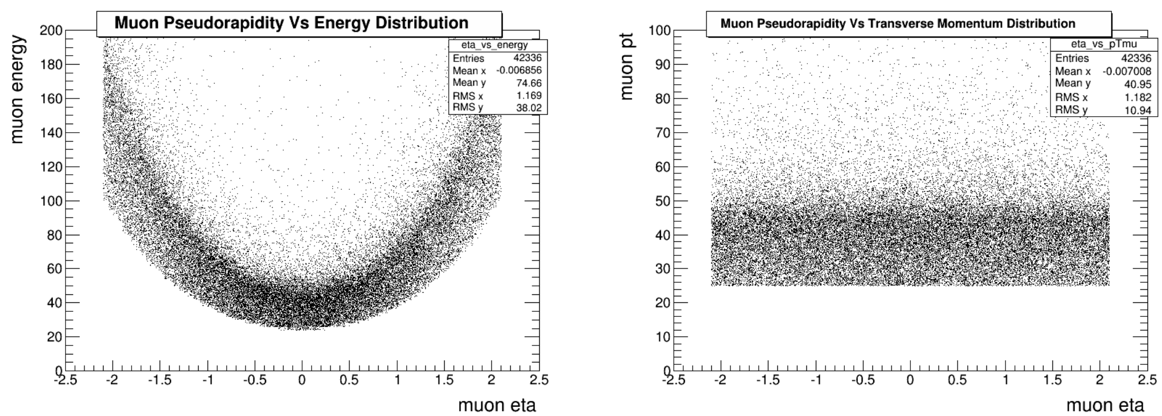

(a) (b)

Figure 4.4: (a) Muon energy as function of pseudorapidity (b) Muon transverse momentum as function of pseudorapidity.

- **Discussion of Plots**

  In Figure 4.4, dependence of muon energy and transverse momentum on muon pseudurapidity was observed. Events with $p_T > 25$ GeV/c and $|\eta| < 2.1$ were selected. By looking at Figure 4.4 (a), it was observed that from endcap towards barrel region, the energy decreased. Most of the muons had energy equal to $(40 - 45)$ GeV as muon density was high in that region. On the other hand, by looking at 4.4 (b), it was observed that transverse momentum of muons was independent of the pseudorapidity of muons. Also muon number density was high in the transverse momentum range (40 − 45) GeV/c so it was understood that momentum of muon about z-axis was dependent on the pseudorapidity of muons (as transverse momentum of muons depends only on p_x and p_y whereas energy depends on p_z also). Also as p_T was independent of η so triggers having p_T cut (not an energy cut which depends upon η) are normally used.

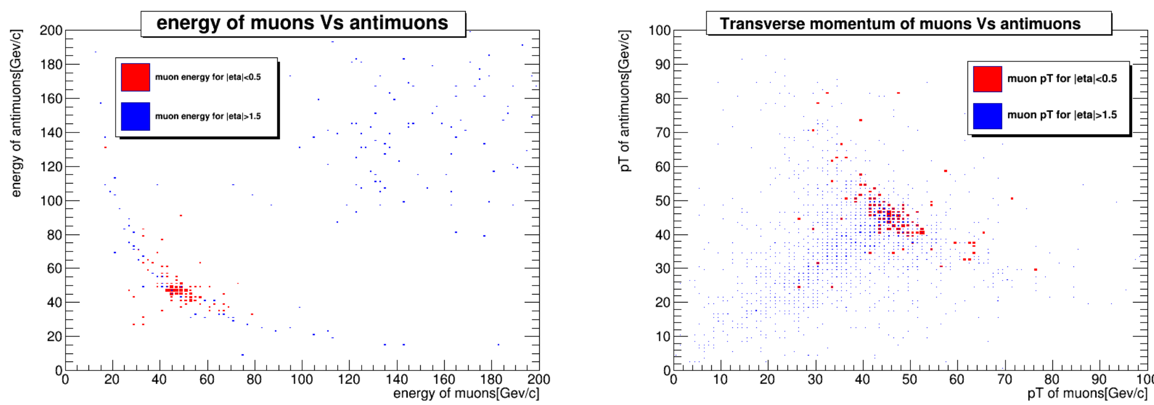

(a) (b)

Figure 4.5: (a) Energy of muons vs energy of antimuons having different pseudorapidity range (b) Transverse momentum of muons vs transverse momentum of antimuons having different pseudorapidity range.

- **Discussion of Plots:**

  In Figure 4.5 (a), a two dimensional plot of energy of muon versus energy of antimuon was observed having different pseudorapidity range. For barrel region (where $|\eta| < 0.5$), most of the muons having energy in the range equals to (40−45) GeV were observed so in barrel region most of the muons were produced from Z boson nearly at rest so it could be assumed that a p_T distribution of Z boson for barrel region muons should be approximately close to zero momentum. Now coming towards endcap ($|\eta| > 1.5$) muons, there were less number of muons having energy equal to 45 GeV but most of the muons had very large amount of energy which meant that the muons detected in endcap region may be produced from Z boson having comparatively high momentum and energy. To see a clear picture, histograms were also normalised to unit area. In Figure 4.5 (b), again for barrel region, most of muons had transverse momentum around 45 GeV/c.

4.3 Background Processes

There are several processes other than $Z \to \mu^+\mu^-$ which can also produce two muons in the final state. These are grouped into three distinct sets:

- Diboson production and decay to muons
- $t\bar{t}$ contribution
- QCD contribution

Datasets listed in Table 4.3 were used to estimate background contribution in signal region. These can be a source of reducible background.

4.3.1 Gauge Bosons Contribution

The processes having dibosons e.g WZ and ZZ although contain real Z boson but these are also considered as background in the analysis. All WZ, ZZ and WW decay processes were produced with Pythia in leading order of α_s. In these processes, the contribution from Z boson can be observed by looking at Z boson mass distribution having a small peak near the Z mass value.

4.3.2 Top Anti-Top Pair Contribution

Top anti-top pair production and decay to muons is also a source of background. Top quark normally decay into a W boson and bottom quarks. W boson can further decay into a muon having probability roughly equal to 11% [38]. 1% of $t\bar{t}$ pair decay to two muons. As both these muons are not created by same mother particle, so the parent particle mass distribution does not show any peak rather it shows a flat distribution.

4.3.3 QCD Contribution

In proton-proton collisions, gluon and quark scattering gives rise to hadronic jets. These jets have a great variety of particles including muons but these muons generally have company of other neutral and charged particles in same direction. By applying a cut on muon transverse momentum $p_T > 25$ GeV/c, we can reduce the amount of fake muons produced by this QCD contribution.

For analysis study, diboson and $t\bar{t}$ background MC files as mentioned in Table 4.3 were used.

4.4 Monte Carlo and Data Samples

The MC and data samples having CMSSW_5_3_2 release version were used for analysis study. Some specifications of data and MC samples are given below.

4.4.1 Signal MC Samples

MC sample is a sample based on theoretical predictions (Standard Model) so if Standard Model is correct and there is no new physics then MC and real data should be in agreement which is the base of any analysis.

The signal MC sample of Summer 2012, at 8 TeV center of mass energy and generated by using "Pythia 6" interfaced with "POWHEG" package was used for analysis study. The signal process was "Drell-Yan process" having lower mass limit on parent particle mass ($M_Z > 20$ GeV/c^2). A subset of this dataset having $\approx$ 1169101 events was processed to work locally. MC was used throughout the analysis for comparison purpose and efficiency measurement e.t.c.

Table 4.2: Signal MC Dataset

File Name	Dataset Path	No. of Events	luminosity	cross section
MC	/DYToMuMu_M-20_ CT10_TuneZ2star_v2_ 8TeV-powheg-pythia6 /Summer12_DR53X-PU_S10_ START53_V7A-v1/AODSIM	1169101	0.61 fb^{-1}	1916 pb

4.4.2 Background MC Samples

The diboson background samples at 8 TeV center of mass energy were produced by "pythia6" and "tauola" whereas $t\bar{t}$ sample was produced by "madgraph" and "tauola". For further information about used samples, see Table 4.3.

Table 4.3: Background MC Datasets

File Name	Dataset Path	No. of Events	luminosity	cross section
TTjets	/TTJets_MassiveBinDECAY_TuneZ2star_8TeV-madgraph-tauola/Summer12_DR53X-PU_S10_START53_V7A-v2/AODSIM	217601	0.966 fb^{-1}	225.225 pb
Diboson	/WZ_TuneZ2star_8TeV_pythia6_tauola/Summer12_DR53X-PU_S10_START53_V7A-v1/AODSIM	251001	11.181 fb^{-1}	22.4486 pb
Diboson	/ZZ_TuneZ2star_8TeV_pythia6_tauola/Summer12_DR53X-PU_S10_START53_V7A-v1/AODSIM	226201	25.046 fb^{-1}	9.0314 pb
Diboson	/WW_TuneZ2star_8TeV_pythia6_tauola/Summer12_DR53X-PU_S10_START53_V7A-v1/AODSIM	229101	39.417 fb^{-1}	5.8123 pb

4.4.3 Data Samples

The real dataset "DoubleMu" Run A datastream of 2012 at 8 TeV center of mass energy and having luminosity equal to 0.82 fb^{-1} was processed for analysis purpose.

Table 4.4: Real Dataset

File Name	Dataset Path	No. of Events	luminosity
Data(AOD)	/DoubleMu/Run2012A-13Jul2012-v1/AOD	4116677	0.82 fb^{-1}

Single muon dataset was also used for efficiency studies.

Table 4.5: Real Dataset

File Name	Dataset Path	No. of Events
Data(AOD)	/SingleMu/Run2012A-13Jul2012-v1/AOD	1162623

4.5 Event Selection

For reco level MC and Data analysis, it was necessary to include proper events first by using filter in the form of a "Trigger" and then proper selection and isolation criteria on the final particles was imposed.

4.5.1 Online Event Selection

Online event selection is based upon the involved muon trigger. Muon trigger selects the event in which a specific value of minimum momentum of muon is mentioned.

In the analysis, events having an "OR" between a single muon and a double muon trigger (as mentioned in Table 4.6) having certain minimum momentum were selected.

Table 4.6: Trigger Selection

No. of Triggers	Selected Triggers
1	$HLT\_IsoMu24\_eta2p1$
2	HLT_Mu17_Mu8

4.5.2 Muon Kinematics

In order to reconstruct Z boson from two muons, it was necessary to select two oppositely charged muons. The threshold of muon momentum $p_T > 25$ GeV/c was applied in the analysis. By applying that minimum momentum cut, the peak at 10 GeV/c in transverse momentum distribution of muons could be avoided which was the contribution due to virtual photons. Furthermore, a cut on pseudorapidity of muons $|\eta| < 2.1$ was also applied.

4.5.3 Muon Reconstruction Criteria

The reconstruction quality criteria of muons was based on the tight muon selection as suggested by "Muon Physics Object Group" [35]. The involved selection cuts are described in following and these are the baseline selection cuts for all muons which are involved in this dissertation.

Muons can be generated by the decays in hadronic flight so these muons are generated within a hadronic jet because of it, these muons have additional energy deposits and tracks and these may not be detected by the inner tracking detector. A cut on number of selected muons by selecting only Particle Flow muons and Global muons is applied. In order to match a track in the tracking system (created by a charged particle) with the track in muon system, the reconstruction quality criteria is usually poor. This quality is measured in terms of χ^2 value of the track fit. A threshold for normalized χ^2 value of track is given by

$$\chi^2/n.d.f < 10$$

By applying this cut, the hadronic punch through can be suppressed and by applying

$$recoMu.innerTrack() \rightarrow hitPattern().numberOfValidPixelHits() > 0$$

muons originating from decay of hadronic flight can be suppressed.

Another cut which was included in tight muon selection is given by

$$recoMu.numberOfMatchedStations() > 1$$

which shows that selected muon should segments in atleast two stations as high energetic jets can produce fake muons jets which can pass through HCAL and solenoid and then can enter to the first muon detector station. The iron return yoke prevents the further penetration into the muon system so by applying above mentioned cut, the number of fake muons can be reduced.

The cuts

$$fabs(recoMu.muonBestTrack() \rightarrow dxy(vertex \rightarrow position())) < 0.2$$

$$fabs(recoMu.muonBestTrack() \rightarrow dz(vertex \rightarrow position())) < 0.5$$

were used to suppress cosmic muons contribution.

For a good transverse momentum measurement the cut

$$track() \rightarrow hitPattern().trackerLayersWithMeasurement() > 5$$

was used which showed the threshold of number of points of measurement in tracker.

4.5.4 Muon Isolation

By applying muon isolation cut, the real and fake muons can be further separated. As color charge is not involved in Z boson decay into two muons so this decay does not involve any hadronic activity due to which the additional tracks and deposited energy around muons is limited.

Following isolation variable cut was applied in the code

$$isolationR03().sumPt < 2.5$$

which basically sums over transverse momentum of all particles in a cone having radius ($R = 0.3$) around the jet containing muon and value of this sum was taken to be less than 2.5 GeV/c to isolate fake muons from real muons.

4.5.5 Pileup Reweighting

The phenomenon in which more than two protons of colliding beams interact with each other is called Pileup and because of this pileup in an event there can be more than one primary vertex. With the increase in the instantaneous luminosity by LHC, pileup also increases so pileup reweighting should be applied while comparing MC with the real data.

In the analysis, first the pileup distributions for MC and real data were obtained. Both distributions were compared and event weights were calculated. After applying event weights to all MC distributions those were compared with the respective data distributions. For further details, see [36].

The distribution of the number of reconstructed primary vertices before and after pileup reweighting is shown in the Figure 4.6.

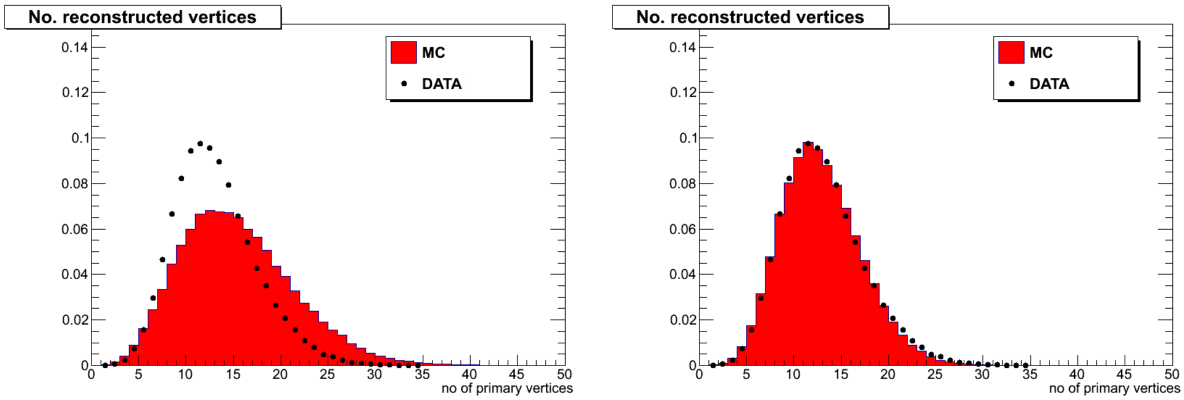

(a) (b)

Figure 4.6: (a) Distribution of number of primary vertices before reweighting (b) Distribution of number of primary vertices after reweighting.

4.5.6 JSON File

It is important to include particular lumi sections for which all parts of CMS detector were in working condition so only those runs should be processed. Files which contain those runs are written in JSON (Java Script Object Notation) format and are called as JSON files (Locate JSON files on [37]). The run range for the used dataset was from 190456 to 193621. Used JSON file should contain this run range.

Table 4.7: JSON File

Used JSON File
$Cert\_190456-196531\_8TeV\_13Jul2012ReReco\_Collisions12\_JSON\_MuonPhys.txt$

4.5.7 Luminosity Calculation

For data and MC comparison purpose, MC was normalised to data luminosity. For that purpose, value of data and MC luminosity was calculated as given below.

The MC luminosity $\mathcal{L}_{MC}$ was calculated by definition

$$\mathcal{L}_{MC} = \frac{no\,of\ events}{cross\ section_{MC}}$$

The total number of MC events processed was 1169101 and the cross section value for the particular signal MC dataset 4.2 listed the CMS twiki page was 1916 pb so the value for luminosity of MC came out to be

$$\mathcal{L}_{MC} = 0.610\ fb^{-1}$$

The data luminosity was calculated by using “lumiCalc2.py”. The value for luminosity of the dataset mentioned in 4.4 came out to be

$$\mathcal{L}_{data} = 0.82\ fb^{-1}$$

Similarly luminosity values for all other background MC datasets were calculated.

4.5.8 Normalization of MC to Data Luminosity

To normalize MC to data luminosity, a scale factor was needed to rescale all kinematic variable plots for MC. The scale factor was calculated by dividing data to MC luminosity having value equal to 1.34. Similarly the scale factors for all background MC samples were calculated and applied to all MC distributions.

4.5.9 Kinematic Variable Distributions for Data and MC

Following plots were obtained after applying all conditions mentioned above.

- **Muon Multiplicity Distribution**

  This plot shows the total number of selected muons in an event. Even number of muons in an event were observed which could reconstruct a Z boson as parent particle. Plot 4.7 represents the same.

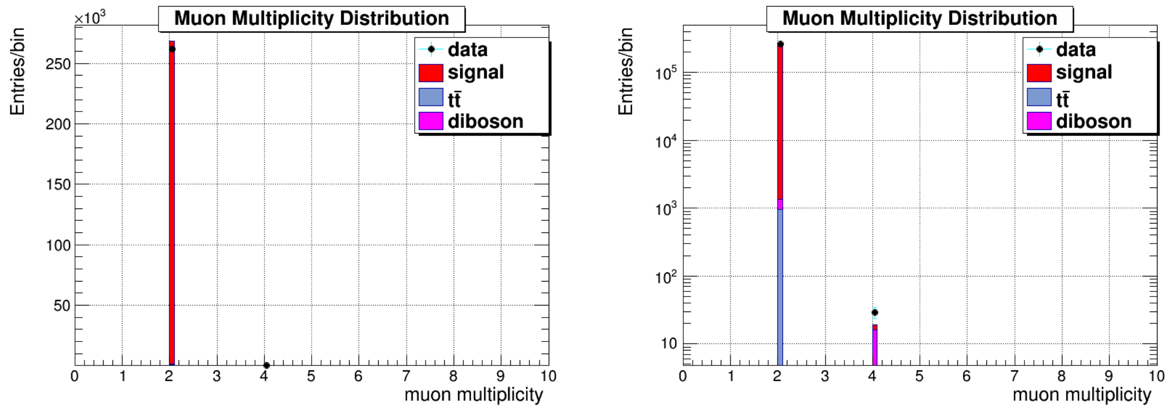

(a) (b)

Figure 4.7: (a) muon multiplicity distribution (b) muon multiplicity distribution having log scale along y-axis.

- **Muon Charge Distribution**

  Muon charge distribution was observed in this plot. Half of the selected final state particles in an event had charge equal to +1 and half of those had charge equal to −1 so there were equal number of muons and antimuons in a particular event.

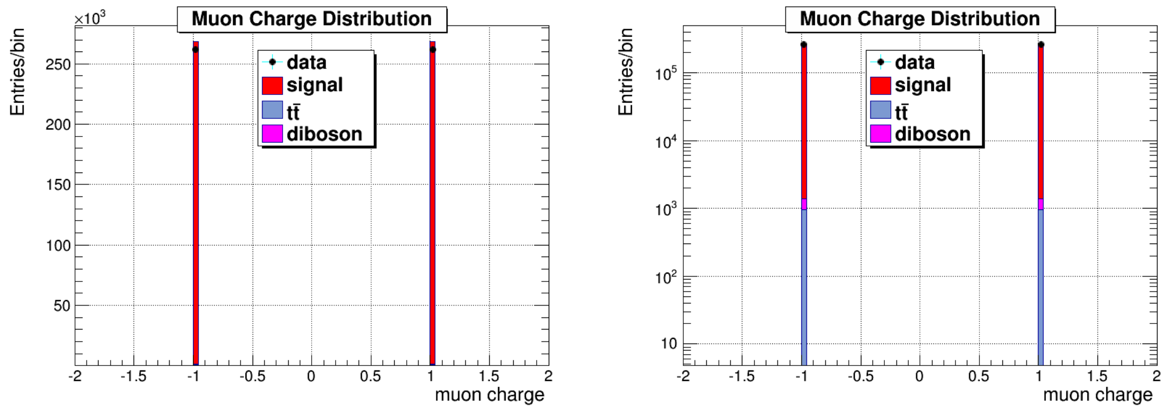

(a) (b)

Figure 4.8: (a) muon charge distribution (b) muon charge distribution having log scale along y-axis.

- **Muon Momentum Distribution Along X-axis**

  A peak was observed in muon momentum distribution close to (± 45 GeV/c) which reflected the fact that the number of muons around that value was much greater than the muons having other momentum values so most of those muons can reconstruct a Z boson at rest.

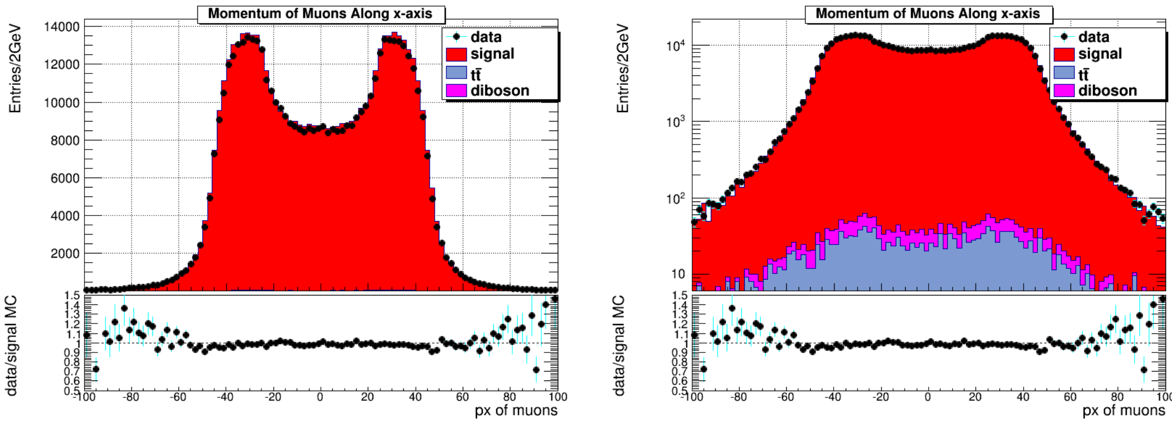

(a) (b)

Figure 4.9: (a) muon momentum distribution along x axis (b) muon momentum distribution along x axis having log scale along y axis.

- **Muon Momentum Distribution Along Y-axis**

  Again a peak was observed around 45 GeV/c value of the muon momentum. The reason was same as described above.

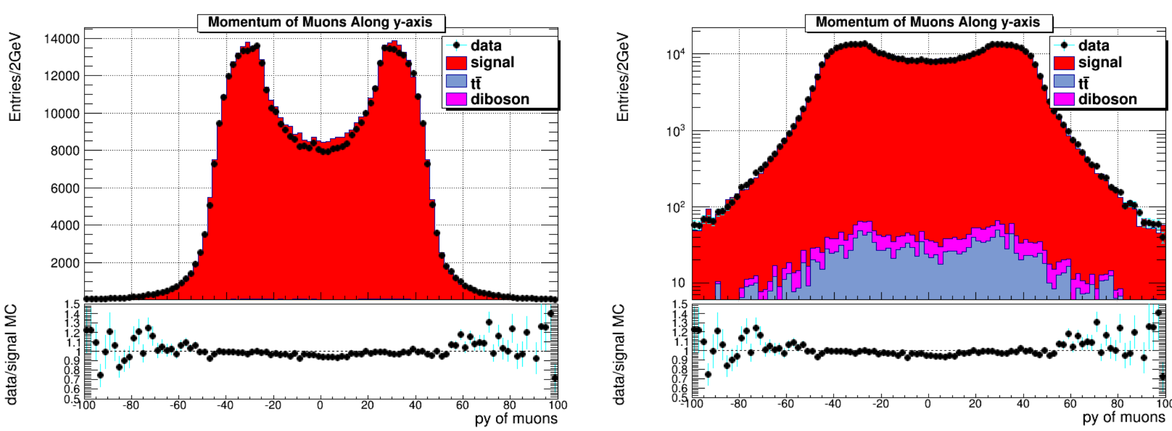

(a) (b)

Figure 4.10: (a) muon momentum distribution along y axis (b) muon momentum distribution along y axis having log scale along y axis.

- **Muon Momentum Distribution Along Z-axis**

  A peak was observed around zero momentum value in the distribution of momentum along z-axis so majority of the selected muons were ejected out in transverse plane rather than parallel plane along beam axis (z-axis).

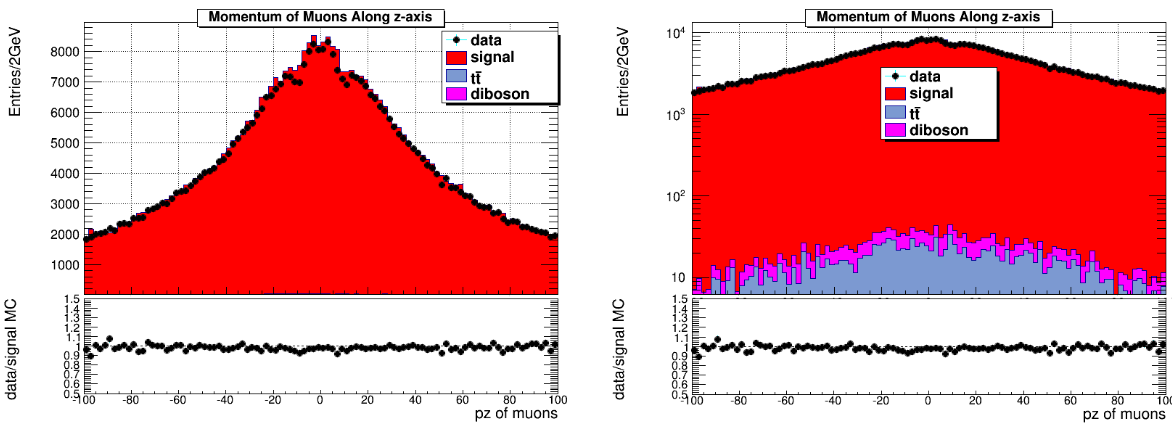

(a) (b)

Figure 4.11: (a) muon momentum distribution along z axis (b) muon momentum distribution along z axis having log scale along y axis.

- **Energy Distribution of Muons**

  In the muon energy distribution, again a peak was observed around 45 GeV and the number of muons having higher energies went on decreasing.

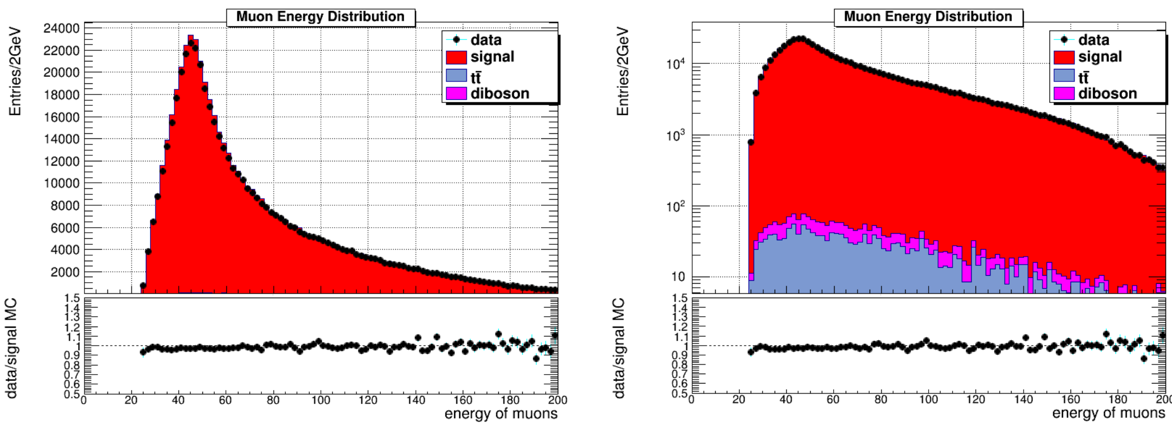

(a) (b)

Figure 4.12: (a) Energy distribution of muons (b) energy distribution of muons having log scale along y axis.

- **Muon Transverse Momentum Distribution**

  The momentum of particles along the transverse plane is known as transverse momentum. It is usually denoted by p_T and it can be calculated as

$$p_T = \sqrt{p_x^2 + p_y^2}$$

  where p_x and p_y are momentum along x and y axis respectively. The transverse momentum distribution was found similar to muon energy distribution having large number of muons around 45 GeV/c momentum. Also a cut at 25 GeV/c was observed which was applied in the selection criteria of muons.

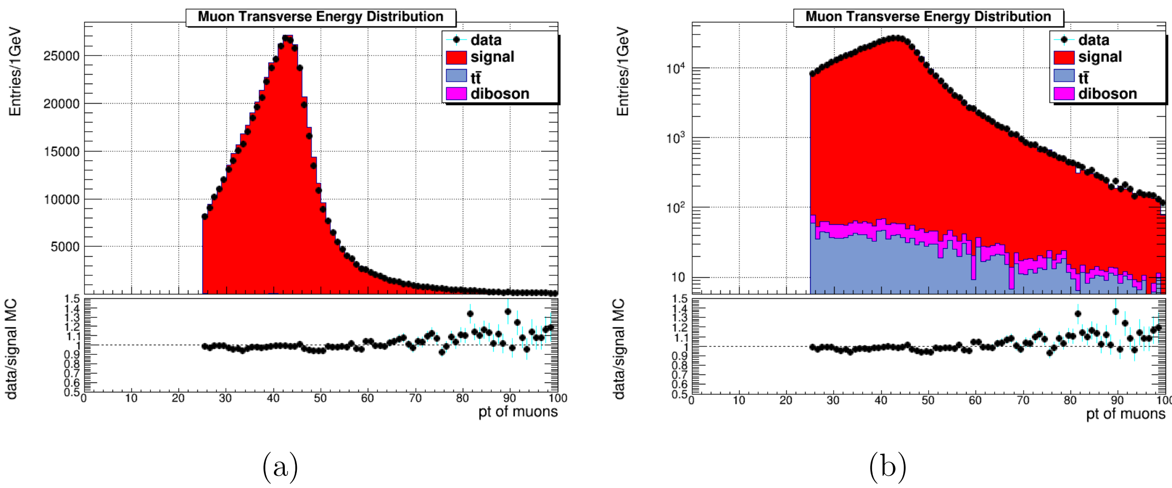

Figure 4.13: (a) muon transverse momentum distribution (b) muon transverse momentum distribution having log scale along y axis.

- **Pseudorapidity Distribution of Muons**

  Pseudorapidity can be defined as

$$\eta = -ln\left(\tan\frac{\theta}{2}\right)$$

  where θ is the angle with respect to beam axis (z-axis).

  The distribution was found symmetric which indicated a good detector.

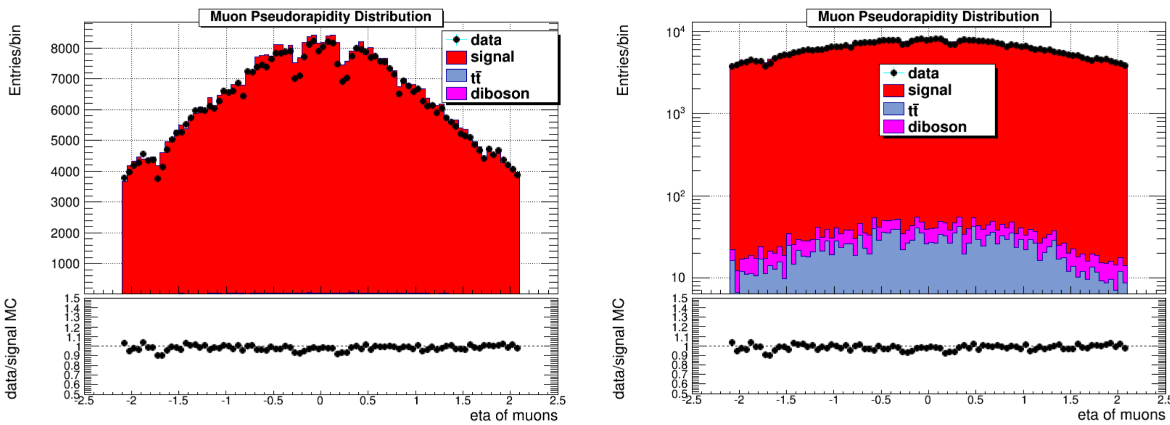

(a) (b)

Figure 4.14: (a) pseudorapidity distribution of muons (b) pseudorapidity distribution of muons having log scale along y axis.

- **Azimuthal Angle Distribution of Muons**

  The angle in transverse plane (xy-plane) starting from x-axis towards y-axis is known as azimuthal angle. Mathematically

$$\phi = tan^{-1}\left(\frac{p_y}{p_x}\right)$$

  The distribution was found symmetric which indicated a good detector.

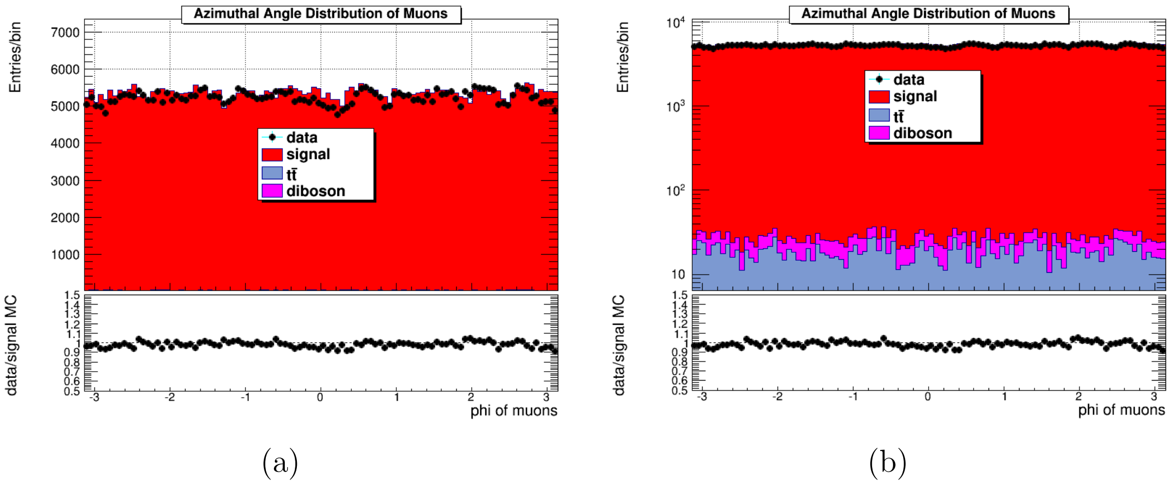

Figure 4.15: (a) azimuthal angle distribution of muons (b) azimuthal angle distribution of muons having log scale along y axis.

- **Pseudorapidity Difference Distribution of Muons**

  The difference of pseudorapidity between muon and antimuon in an event was indicated by this plot. The majority of the muons had delta eta equal to zero which corresponded to theta equal to 90^0 so those muons were emitted in the transverse plane.

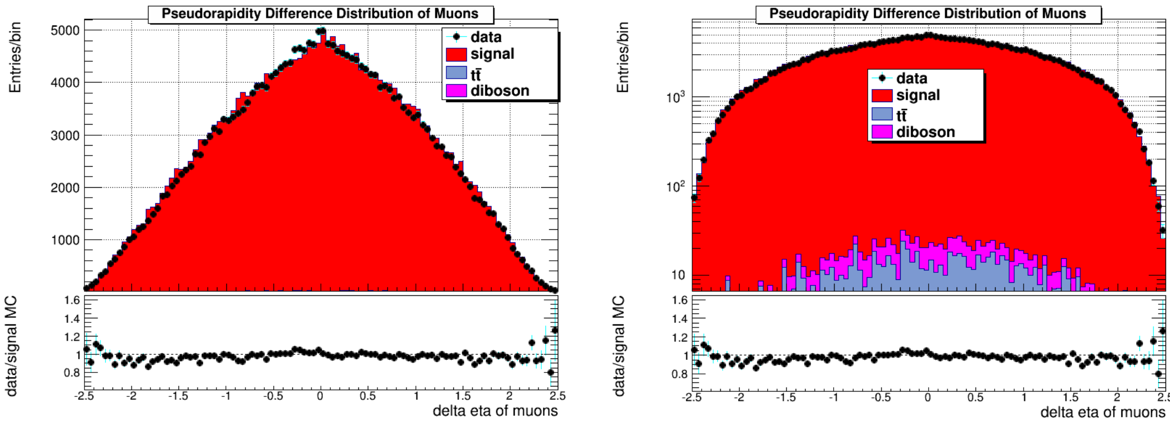

(a) (b)

Figure 4.16: (a) pseudorapidity difference distribution of muons (b) pseudorapidity difference distribution of muons having log scale along y axis.

- **Azimuthal Angle Difference Distribution of Muons**
  Azimuthal angle difference distribution is represented in the plot. Majority of the muons were observed to have value equal to ± 3.14 radian (which corresponds to 180^0 angle) which basically represented the back to back muon emission so Z pt distribution was expected to have peak near zero GeV/c. A small peak at zero value of delta phi in data was observed which may be due to QCD background.

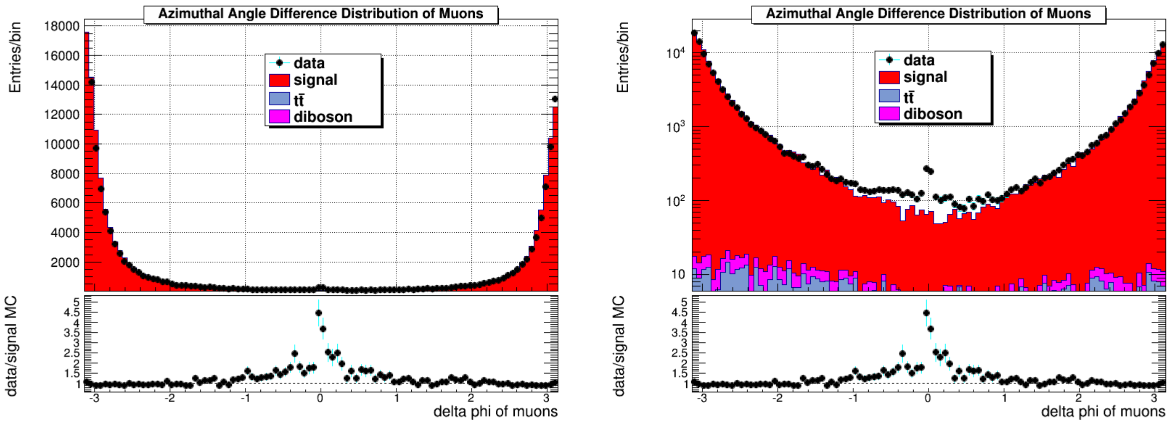

(a) (b)

Figure 4.17: (a) azimuthal angle difference distribution of muons (b) azimuthal angle difference distribution of muons having log scale along y axis.

- **Transverse Momentum Distribution of Reconstructed Z boson**

  As discussed before, most of reconstructed Z bosons were found to have transverse momentum nearly equal to zero because these were created at rest by the reconstruction of two back to back muons. The distribution was obtained by using following formula

$$Zp_T = \sqrt{(px_1 + px_2)^2 + (py_1 + py_2)^2}$$

  where px_1 and px_2 denote the momenta along x-axis for muon and antimuon respectively. Similarly py_1 and py_2 denote the momenta along y-axis for muon and antimuon.

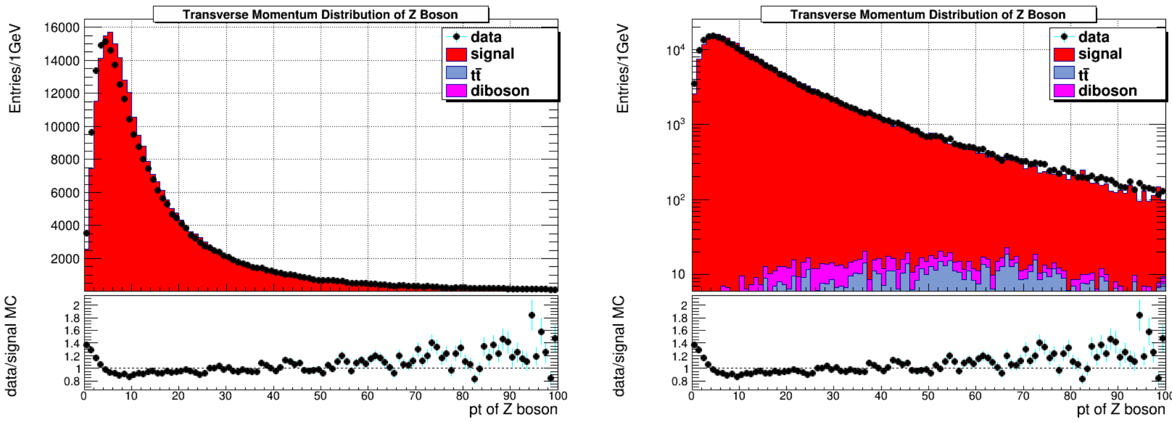

(a) (b)

Figure 4.18: (a) transverse momentum distribution of Z boson (b) transverse momentum distribution of Z boson having log scale along y axis.

- **Z boson Mass Distribution**

  By reconstruction of the muon and antimuon in an event, mass of the parent particle was obtained by using following formula

$$M_Z = \sqrt{(e_1 + e_2)^2 - \{(px_1 + px_2)^2 + (py_1 + py_2)^2 + (pz_1 + pz_2)^2\}}$$

  where e_1 and e_2 denotes energy of muon and antimuon in an event respectively and other terms denote the same as described previously.

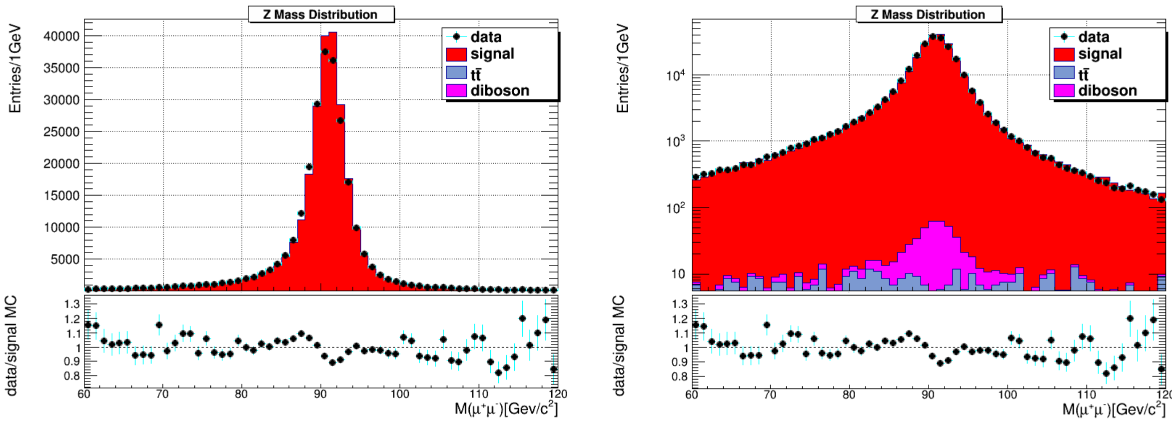

(a) (b)

Figure 4.19: (a) Z mass distribution (b) Z mass distribution having log scale along y axis.

The number of entries in Z mass plot for data were noted as mentioned below

$$N_{obs} = 261778 \tag{4.5.1}$$

4.6 Z Boson Mass Peak Fitting

For fitting Z mass peak, convolution of Relativistic Breit Wigner distribution and Crystal Ball function was used. By definition, Relativistic Breit Wigner distribution is

$$BW(m; M_Z, \Gamma_Z) = \frac{\Gamma_Z^2 m^2 / M_Z^2}{(m^2 - M_Z^2)^2 + \Gamma_Z^2 m^4 / M_Z^2}$$

where m is mass of resonance, Γ is decay width and M_Z is the Z boson mass. Crystal ball function is defined as

$$CB(x; \alpha, n, \mu, \sigma) = \begin{cases} exp\left(\frac{-(x-\mu)^2}{2\sigma^2}\right) & \text{for } \frac{(x-\mu)}{\sigma} > -\alpha \\ A.\left(B - \frac{(x-\mu)}{\sigma}\right)^{-n} & \text{for } \frac{(x-\mu)}{\sigma} \leq -\alpha \end{cases}$$

where

$$A = \left(\frac{n}{|\alpha|}\right)^n .exp\left(\frac{-|\alpha|^2}{2}\right) \quad and \quad B = \frac{n}{|\alpha|} - |\alpha|$$

where x, α, n, μ and σ are parameters of crystal ball function fitted with data.

Two parameters (i.e mass of Z boson and width of Z boson mass distribution to 91.1876 and 2.4952 respectively) were fixed for the analysis. The fit window was taken from $(80 - 100)$ GeV/c^2 and the plot obtained is shown in Figure 4.20.

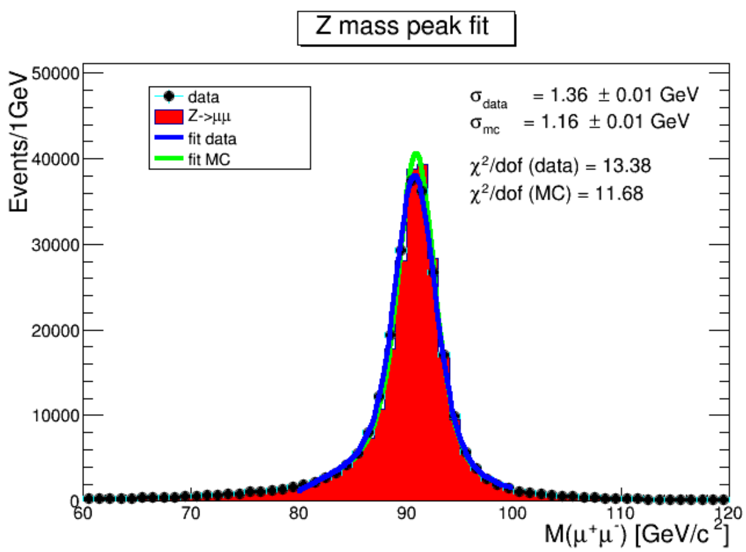

Figure 4.20: Z mass peak fit plot

4.7 Background Estimation

The number of background events was calculated by using two methods.

- **By Adding all Background MC Samples**
- **By Fit Method**

4.7.1 By Adding all Background MC Samples

For calculating number of background events accurately, the number of entries in Z mass plot (obtained by adding all Z mass histograms from all MC background datasets one by one) were noted. The combined histogram, after adding all background contributions (except QCD, which would not effect the distribution much) and after normalizing all MC to data luminosity, can be observed in Figure 4.21.

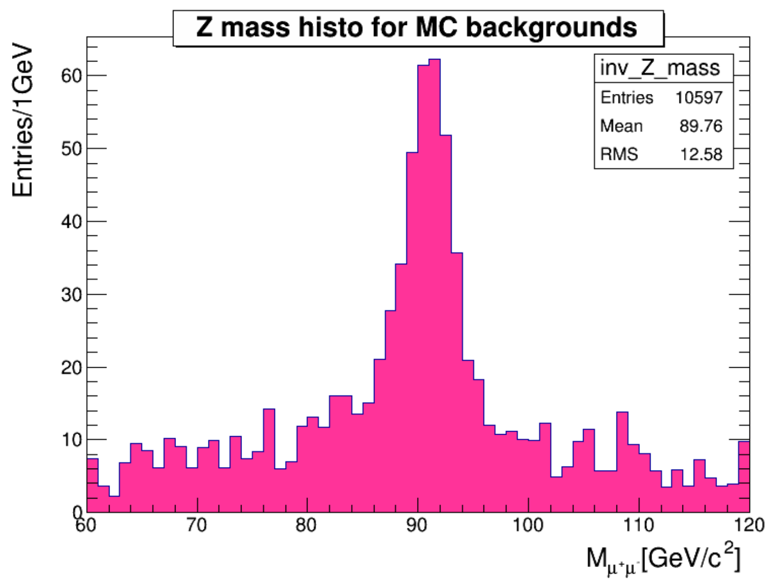

Figure 4.21: Combined Z mass plot for backgrounds

The number of background events were noted having value equal to 10597 (excluding QCD contribution).

4.7.2 By Fit Method

In this method, Z mass peak using "RooFit" (for details, see [39]) was fitted. For signal region, Gaussian function [40] convoluted with the Breit Wigner distribution was used and for background region, exponential function was used. The addition of all three above mentioned fit functions is represented by the global fit. In Figure

4.21, the "nbackground" count represents the number of background events in data which lie under the exponential curve.

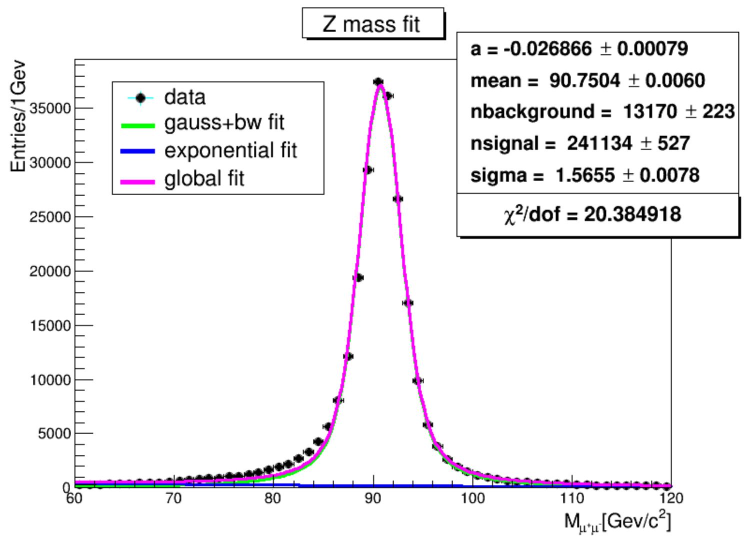

Figure 4.22: Gauss+BW+expo fit of data

The number of background events was equal to 13170 which was close to the number previously obtained by adding all MC background samples (Note that this number also includes QCD events so it is greater than the previous number) so it can be written as

$$N_{bkg} = 13170 \pm 223 \tag{4.7.1}$$

4.8 Tag and Probe Method

The efficiency measurements using tag and probe method is a developed procedure within HEP. This method gives an unbiased estimate and is applicable to both MC and data. Well known resonances such as J/ψ and Z are exploited by tag and probe method.

By using tag and probe method, firstly $Z \to \mu^+\mu^-$ candidates with asymmetric selection criterion for two daughter particles (muons) were selected. The particle which passed a very tight selection criteria and also a trigger selection criteria is called as a "Tag". The other particle called "Probe" was selected having loose selection cuts (The selection for probe is somewhat relaxed) and for trigger efficiency measurement, the ratio of probes which passed certain trigger to the probes which did not pass the trigger was calculated. A constraint of invariant mass of both daughter particles in certain range was also applied which was the requirement for parent particle mass.

4.8.1 Measurement of Trigger Efficiencies

Trigger plays a very important role in many analyses including Z boson cross section measurements. An inefficient trigger can effect our event selection and consequently final analysis. To be an efficient trigger, the efficiency of the trigger should be high (close to one).

The implication of the trigger in any analysis is based on different steps. The first step is called "Level 1 Trigger" which is used in detector hardware which shrinks events from several millions to several thousands per seconds. Then the events are processed by using software called as "High Level Trigger (HLT)". This trigger applies cuts on kinematic variables of trigger objects for example on particle pseudorapidity or transverse momentum (see Table 4.6). This is divided into "Level 2" and "Level 3" triggers. Level 2 works on calorimeter and muon system whereas Level 3 trigger also performs track reconstruction.

For trigger efficiency measurement in the analysis, tag and probe method was used. First, a muon (tag) with tight ID cuts as suggested by Muon POG group was selected. Then a second muon (probe) which when combined with the tag, gave invariant mass in the range $(80 - 100)$ GeV/c^2 (close to Z boson mass) was selected then the further selection cuts on probe were also applied. First, all the steps were performed without including any trigger in the event and then trigger was also included. By taking ratio of the muon p_T and η plot with trigger to the muon p_T and η plot without trigger, trigger efficiency distribution was obtained. The plots obtained are shown in figure 4.23.

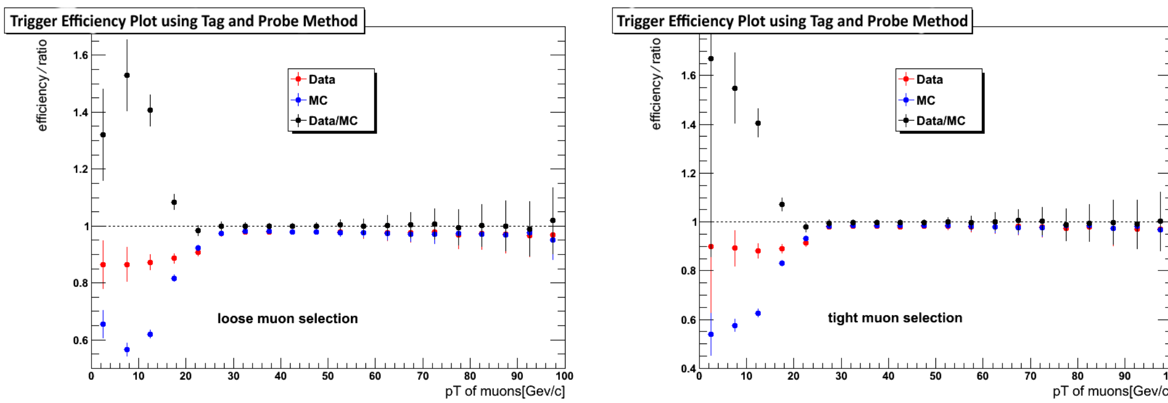

(a) (b)

Figure 4.23: (a) Trigger efficiency plot using DoubleMuon datastream and using "$HLT\_IsoMu24\_eta2p1\ OR\ HLT\_Mu17\_Mu8$" trigger and selecting loose ID probe muons (b) Trigger efficiency plot using DoubleMuon datastream and using "$HLT\_IsoMu24\_eta2p1\ OR\ HLT\_Mu17\_Mu8$" trigger and selecting tight ID probe muons.

Double muon dataset was used in above plots and the used trigger was an "OR" between single muon and a double muon trigger. It can be observed that the selection criteria of the probe does not effect the efficiency plot much so it is possible to have probe having somewhat relaxed cuts values. Also it can be observed that an "OR" trigger was very efficient trigger having efficiency almost equal to one but as Double muon datastream was used, the results were biased. To obtain unbiased results, Single muon datastream was used further for efficiency studies.

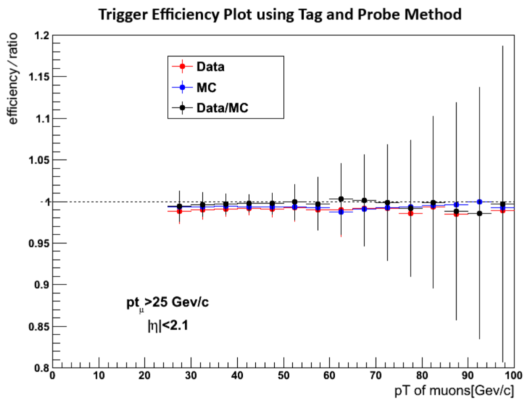

(a)

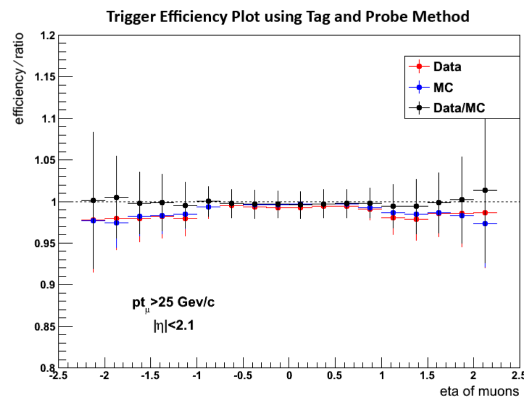

(b)

Figure 4.24: (a) Trigger efficiency as function of transverse momentum of muons using double muon datastream having cuts on p_T and η of muons (b) Trigger efficiency as function of pseudorapidity of muons using double muon datastream having cuts on p_T and η of muons.

The dependence of efficiency on the transverse momentum and pseudorapidity of muons using double muon datastream for trigger and having an "OR" between double muon trigger and single muon trigger was observed. After applying cuts on transverse momentum of muons $p_T > 25$ GeV/c and on muon pseudorapidity $|\eta| < 2.1$, efficiency was found almost equal to one so used trigger was an efficient trigger.

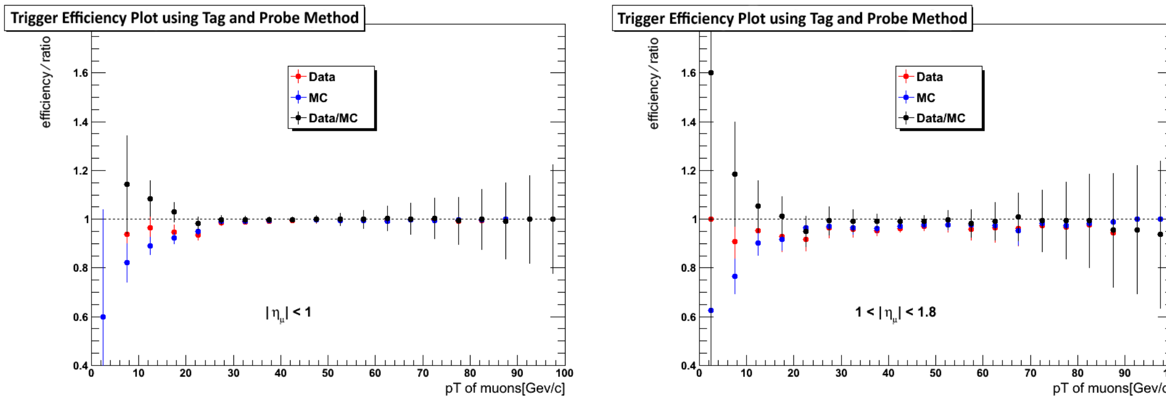

(a) (b)

Figure 4.25: (a) Trigger efficiency plot using double muon datastream selecting barrel muons only $|\eta_\mu| < 1$ (b) Trigger efficiency plot using double muon datastream selecting endcap muons $1 < \eta_\mu| < 1.8$.

Barrel muons were observed to have trigger efficiency almost 100% whereas endcap muons were observed to have trigger efficiency nearly 95%.

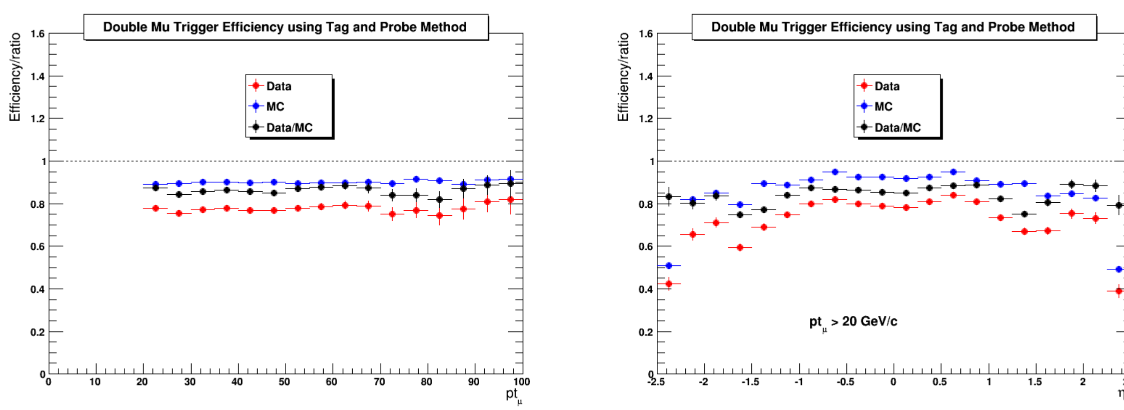

(a) (b)

Figure 4.26: (a) Trigger efficiency as function of p_T of muons using single muon datastream selecting only double muon trigger (b) Trigger efficiency as function of η of muons using single muon datastream selecting only double muon trigger.

Unbiased results were obtained using Single muon datastream. In addition to Single muon datastream, only double muon trigger (i.e HLT_Mu17_Mu8) was used. A discrepancy between data and MC was observed. MC trigger efficiency was nearly equal to $(91-92)\%$ but data efficiency was much smaller almost $(78-79)\%$. It could be because of more background in data. So,

$$\mathcal{E}_{trig} = 0.79 \tag{4.8.1}$$

4.8.2 Measurement of Muon Tight ID Efficiency

Muon tight ID efficiency was calculated using Tag and Probe method as described earlier. The tight ID selection cuts as suggested by Muon POG group were tested and found efficient. The procedure adopted to calculate tight ID efficiency is described below.

First in an event, a tight muon (tag) was selected. Then another muon that together with the tag could produce invariant mass in $(80-100)$ GeV/c^2 window was selected. Then tight selection cuts were applied on the probe also. The p_T and η distributions of the probe were obtained. Again same procedure was repeated but at this time, no selection cuts on probe were applied. Again p_T and η distributions of the muons were obtained. By taking the ratio of first p_T/η plot to second p_T/η plot, the tight ID efficiency plot was obtained which informed us about the number of probes which satisfy tight selection cuts.

The Single muon datastream was used and no trigger was applied for calculating tight ID efficiency. Tight ID efficiency was also found close to 90%. Following plots were obtained.

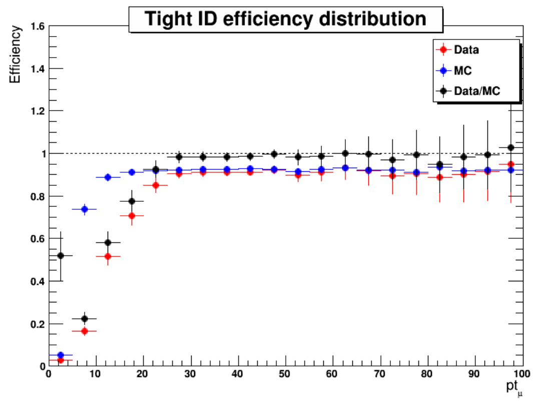

(a)

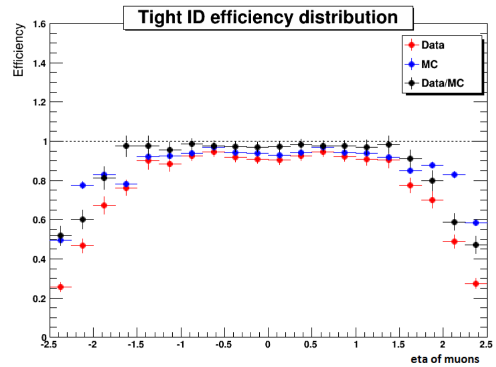

(b)

Figure 4.27: (a) Tight ID efficiency as function of p_T of muons using single muon datastream (b) Tight ID efficiency as function of η of muons using single muon datastream.

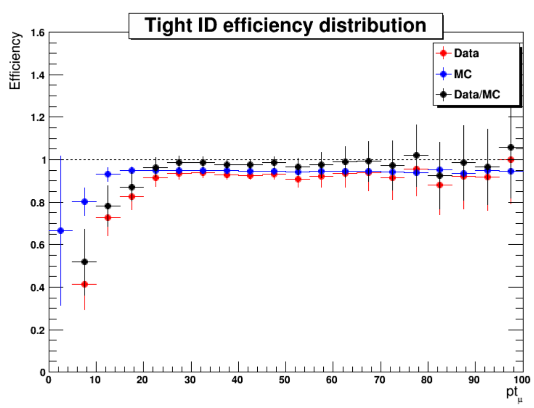

(a)

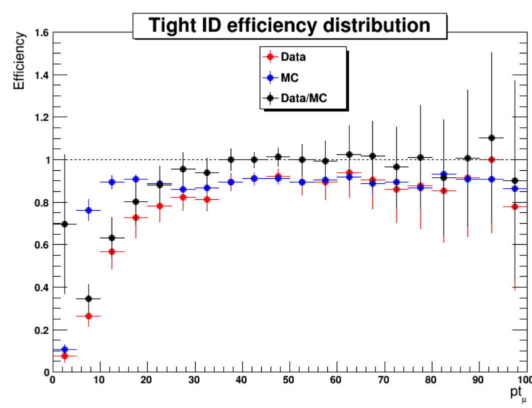

(b)

Figure 4.28: (a) Tight ID efficiency selecting barrel muons using single muon datastream (b) Tight ID efficiency selecting endcap muons using single muon datastream.

The calculated value for selection (tight ID) efficiency was

$$\mathcal{E}_{sel} = 0.92 \tag{4.8.2}$$

4.9 Muon Momentum Scale and Resolution

It is always very difficult to measure something accurately. In CMS detector, when a muon is observed in a tracker, some flaws and imperfections may have created in measuring the curvature of tracks formed by muons. On the other hand, inaccurate measurement of the magnetic field may also effect the muon momentum value. Also the material from which detector was made and the misalignment of the detector parts may also effect the path of muons so we need to apply muon momentum scale and resolution correction. After applying p_T correction, some differences can still be observed in data and MC resolution. To remove this mismatch, MC smearing should also be added.

"MuScleFit" package was used to apply p_T and smearing corrections in the analysis. The non CMSSW version of MuScleFit package as suggested by [41] was used. Standard values for p_T and smearing were used. The plots before and after corrections are shown in Figure 4.29. Plots were found consistent with the results obtained by CMS (see [42] for more details).

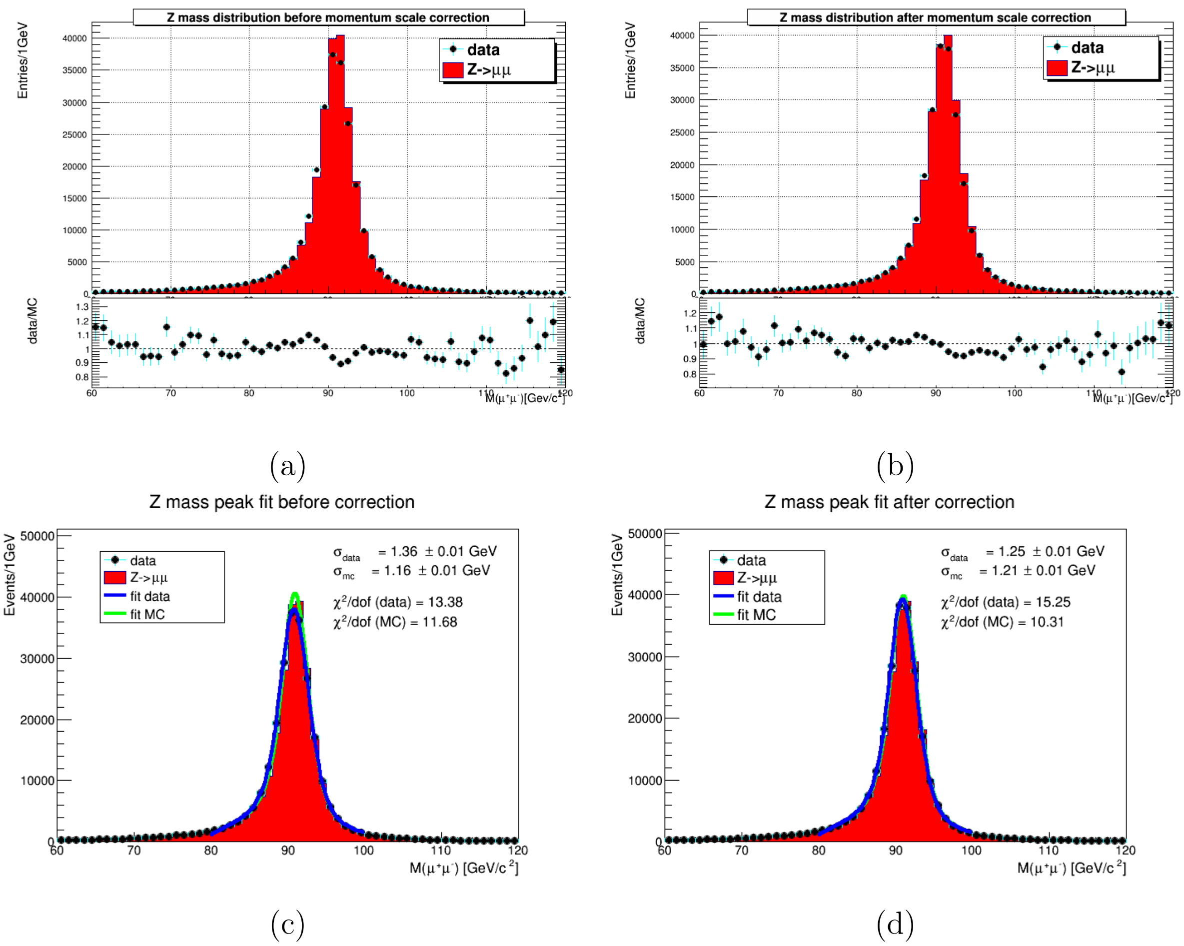

Figure 4.29: (a) Z mass distribution before applying muon p_T correction (b) Z mass distribution after applying muon p_T correction (c) resolution before correction (d) resolution after correction.

4.10 Muon Performance

In section 4.8, various trigger efficiencies were calculated. In some distributions only double muon trigger was used and in others, the efficiencies of double muon "OR" single muon trigger were obtained. By using double muon trigger, the efficiency was less (of about 80%) as compared to the efficiency from an "OR" between single and

double muon trigger (about 100%).
Also the impact of selecting probe muon having tight selection cuts and loose selection cuts, was studied and in both cases, results were found almost similar which indicated that selection of a tight or loose probe did not have much impact.
The impact of selecting double muon and single muon datastream was also studied. By using double muon datastream, biased results were obtained (having efficiency almost 100%) whereas by using single muon datastream unbiased results were obtained (having efficiency of about 80%).
Other than that, efficiency distribution evolution was observed when different p_T and η cuts on muons were applied (see Figure 4.24 and distribution evolution was also observed when barrel or endcap muons were selected (see Figure 4.25).

In section 4.9, the Z mass distribution evolution by applying muon momentum correction and smearing was studied. After applying correction, the discrepancy between data and MC Z mass peak was minimized.

By doing above mentioned steps, the muon performance in the CMS detector was studied.

4.11 Acceptance Calculation

By acceptance $\mathcal{A}$ we mean to calculate the number of events which accept the particular cuts at the generator level.

For calculating value of acceptance, the number of entries were noted in the Z mass plot without including any cut on muon p_T and η and allowing entries to fall in the range $(60 - 120)$ GeV/c^2. Then cuts were included ($p_T > 25$ GeV/c and $|\eta| < 2.1$) and entries were allowed to fall in $(60 - 120)$ GeV/c^2 and then the ratio of 2^{nd} to 1^{st} plot number of entries was calculated to obtain acceptance value. The acceptance value came out to be

$$\mathcal{A} = \frac{239754}{670306} = 0.357 \tag{4.11.1}$$

4.12 Cross Section Measurement

The measurement of cross section directly gives us the probability of occurrence of a certain process. By getting the large value for production cross section of Z boson, we mean to say that Z boson can be easily created, observed and measured. The formula for calculating cross section is given by

$$\sigma_{prod} = \frac{N_{obs} - N_{bkg}}{\mathcal{E}_{trig}.\mathcal{E}_{sel}.\mathcal{A}.\mathcal{L}}$$

where N_{obs} and N_{bkg} are number of observed events after applying all selection cuts and number of background events respectively. $\mathcal{E}_{trig}$, $\mathcal{E}_{sel}$, $\mathcal{A}$ and $\mathcal{L}$ are values of trigger efficiency, selection efficiency (tight ID), acceptance and data luminosity respectively.

After putting value of N_{obs} from Eq.(4.5.1), value of N_{bkg} from Eq.(4.7.1), value of $\mathcal{E}_{trig}$ from Eq.(4.8.1), value of $\mathcal{E}_{sel}$ from Eq.(4.8.2), value of $\mathcal{A}$ from Eq.(4.11.1) and value of $\mathcal{L}$ from Table 4.4, the value for Z boson production cross section was calculated as

$$\sigma_{prod} = \frac{(261778 - 13170)}{(0.79 \times 0.92 \times 0.357 \times 820\, pb^{-1})}$$

$$\sigma_{prod} = 1168\, pb$$

4.13 Cross section Error Calculation

In physics, the result of any experiment without quoting an error is considered to be ambiguous so in this case, the cross section error value must also be reported. As cross section depends upon many quantities, each one of which also have error present in it individually so to calculate error present in total cross section value, we need to take all parameters error into account. Error in each quantity was calculated as given below

- Error in observed number of events N_{obs} after applying all selection cuts denoted by δN_{obs} was calculated as

$$\delta N_{obs} = \sqrt{N_{obs}}$$

$$\delta N_{obs} = \sqrt{261778} = 511.64$$

- Error in background value N_{bkg} denoted by δN_{bkg} was calculated as

$$\delta N_{bkg} = \sqrt{N_{bkg}}$$

$$\delta N_{bkg} = \sqrt{13170} = 114.76$$

- Error in trigger efficiency $\mathcal{E}_{trig}$ denoted by $\delta\mathcal{E}_{trig}$ was calculated by using binomial error calculation formula as given by

$$\delta\mathcal{E}_{trig} = \sqrt{\frac{\mathcal{E}_{trig}(1-\mathcal{E}_{trig})}{N}}$$

where N in the denominator corresponds to measure the number of events without having trigger. After putting values, we obtained

$$\delta\mathcal{E}_{trig} = \sqrt{\frac{0.79(1-0.79)}{29642}} = 0.00237$$

- Error in selection efficiency $\mathcal{E}_{sel}$ denoted by $\delta\mathcal{E}_{sel}$ was calculated by using binomial error calculation formula as given by

$$\delta\mathcal{E}_{sel} = \sqrt{\frac{\mathcal{E}_{sel}(1-\mathcal{E}_{sel})}{N}}$$

where N in the denominator corresponds to measure the number of events without passing selection criteria. After putting values, we obtained

$$\delta\mathcal{E}_{sel} = \sqrt{\frac{0.92(1-0.92)}{34691}} = 0.00147$$

- The error in acceptance value $\mathcal{A}$ denoted by $\delta\mathcal{A}$ was again calculated by using binomial error formula as acceptance is also a parameter like efficiency (as it is a ratio of two quantities) as

$$\delta\mathcal{A} = \sqrt{\frac{\mathcal{A}(1-\mathcal{A})}{N}}$$

where N is number of events without having any p_T and η cut. After putting values, we obtained

$$\delta\mathcal{A} = \sqrt{\frac{0.357(1-0.357)}{670306}} = 0.000585$$

- The uncertainty in luminosity value was quoted from CMS draft analysis note [43] equal to 5%
The final value of uncertainty in luminosity value was calculated as

$$\delta\mathcal{L} = 0.05 \times 0.82 = 0.041 pb^{-1}$$

After calculating the error in all parameters used in cross section formula, the error in the cross section measurement itself was calculated as described below.
While adding or subtracting two quantities, the error or uncertainty itself gets added so a new term defined as δN was the combined uncertainty of δN_{obs} and δN_{bkg}.

$$N \pm \delta N = (N_{obs} \pm \delta N_{obs}) - (N_{bkg} \pm \delta N_{bkg})$$

$$N \pm \delta N = (261778 \pm 511.64) - (13170 \pm 114.76) = 248608 \pm 626.4$$

While multiplying or dividing quantities with uncertainties as given in cross section formula, the uncertainty in cross section value denoted by $\delta\sigma_{prod}$ was calculated as

$$\delta\sigma_{prod} = \sigma\sqrt{\left(\frac{\delta N}{N}\right)^2 + \left(\frac{\delta\mathcal{E}_{trig}}{\mathcal{E}_{trig}}\right)^2 + \left(\frac{\delta\mathcal{E}_{sel}}{\mathcal{E}_{sel}}\right)^2 + \left(\frac{\delta\mathcal{A}}{\mathcal{A}}\right)^2 + \left(\frac{\delta\mathcal{L}}{\mathcal{L}}\right)^2}$$

After putting values, we obtained

$$\delta\sigma_{prod} = 1168\sqrt{\left(\frac{626.4}{248608}\right)^2 + \left(\frac{0.00237}{0.79}\right)^2 + \left(\frac{0.00147}{0.92}\right)^2 + \left(\frac{0.000585}{0.357}\right)^2 + \left(\frac{0.041}{0.82}\right)^2}$$

$$\delta\sigma_{prod} = 58.64$$

So the final value of Z boson production cross section can be written as

$$\sigma_{prod} = 1168 \pm 58.64\ pb \approx 1.17 \pm 0.06\ (stat, lumi)\ nb$$

which was in agreement with the recently published result [43] where the calculated value of cross section was

$$\sigma_{Z\to l^+l^-} = 1.12 \pm 0.01\ (stat.)\ \pm 0.02\ (syst.)\ \pm 0.06\ (lumi.)\ nb$$

Due to time constraint, we were unable to calculate systematic uncertainty. By systematic uncertainty we mean to check the systematic effects in measurements. To calculate systematic uncertainty, the following steps could be done:

- Increase (40−140) or decrease (80−100) the Z mass window to see the impact on systematics
- Increase or decrease the value of p_T and η cuts and see its impact
- Study the impact of including different triggers. Its impact on trigger efficiency could be studied
- Fit Z mass plot by use of different functions e.g Crystal Ball, Breit Wigner and Gaussian and study the difference in number of signal events
- Fit background by exponential and polynomial functions e.t.c

By doing above steps, the value for the systematic uncertainty could be obtained which was separately mentioned in final value of cross section in published Analysis note [43].

Conclusion

In this thesis, measurement of the Z boson production cross section in muon decay channel using 2012 data collected from CMS detector at center of mass energy of 8 TeV having data luminosity equal to 0.82 fb^{-1} is presented. The muon selection criteria as suggested by muon "Physics Object Group" at CERN was adopted for study. Various tools and techniques including generator level study, MC and data reconstruction level study, implication of different selection cuts, pileup reweighting technique, luminosity calculation, comparison of simulation and data, Z mass peak fitting, use of tag and probe method for calculation of trigger and selection efficiency, acceptance calculation were employed to measure Z boson production cross section.

Z boson cross section in muon decay channel (within Z peak $60 < M_Z < 120$) was measured to be (1.17±0.06) nb which includes both luminosity and statistical uncertainty and it was found in agreement with the results presented by CMS in June 2012 [43] having 18.8 pb^{-1} luminosity.

Muon performance was studied in terms of trigger performance and muon momentum and scale resolution and its effects. To check trigger performance, different single and double muon triggers were applied and efficiencies were calculated. To get unbiased results, single muon datastream was also processed and the impact of selecting loose and tight, barrel and endcap muons was studied.

Bibliography

[1] Rudolf Lobl. Demokrits Atomphysik. Ertrage der Forschung ; 252. Wiss. Buchges., Darmstadt, 1987.

[2] Joseph John Thomson. On the structure of the atom: an investigation of the stability and periods of oscillation of a number of corpuscles arranged at equal intervals around the circumference of a circle; with application of the results to the theory of atomic structure. *Philosophical Magazine*, 7(39):237265, 1904.

[3] Helicity in Quantum electrodynamics
"http://www.cft.edu.pl/~birula/sem/Helicity.pdf"

[4] Abelian groups
"http://designtheory.org/library/encyc/topics/abelian.pdf"

[5] Study of Z Boson Decays into Pairs of Muon and Tau Leptons with the CMS Detector at the LHC
Dipl.-Phys. Manuel Zeise, 15 July 2011

[6] Hypercharge and weak isospin
"http://math.ucr.edu/home/baez/qg-spring2003/hypercharge/hypercharge.pdf"

[7] Neutrino Oscillations and Neutrino Mass
"http://www.ps.uci.edu/~superk/nuosc.html"

[8] International Masterclasses Hands on Paticle Physics. The Z boson "https://kjende.web.cern.ch/kjende/en/zpath_zboson.html".

[9] NASA's HEASARC: Education & Public Information "http://heasarc.gsfc.nasa.gov/docs/snr.html"

[10] Welcome to the Worldwide LHC Computing Grid "http://wlcg.web.cern.ch/"

[11] The official String Theory website "http://www.superstringtheory.com/"

[12] Dark Energy, Dark Matter "http://science.nasa.gov/astrophysics/focus-areas/what-is-dark-energy/"

[13] Grand Unified Theories "http://pdg.lbl.gov/2010/reviews/rpp2010-rev-guts.pdf"

[14] The TOTEM Collaboration. The totem experiment at the cern large hadron collider. Journal of Instrumentation, 3(08):S08007, 2008.

[15] A NEW PHYSICS THEORY FUNDAMENTALLY UNIFIED, James A. Putnam, 2011

[16] Extra dimensions "http://theory.uchicago.edu/~smaria/lisa.pdf"

[17] A Supersymmetry Primer, Stephen P. Martin, version 6, September 2011 "http://arxiv.org/pdf/hep-ph/9709356v6.pdf"

[18] Heavy-ion collisions and quark-gluon plasma, past, present and future "http://personalpages.to.infn.it/~nardi/QGPSchool/5th/welc11.html"

[19] Collisions
"http://lhc-machine-outreach.web.cern.ch/lhc-machine-outreach/collisions.html"

[20] Lyndon Evans et al. LHC Machine. JINST, 3:S08001, 2008.

[21] "An Examination of Backgrounds to Early-run Minimum-bias Events in ATLAS at the LHC" by "Alden Reid Stradling"

[22] Austin Ball, Michel Della Negra, L Fo'a, and Achille Petrilli. CMS technical design report, volume II: Physics performance. J. Phys., G34:9951579, 2007.

[23] Impact Parameter for Nuclear Scattering
"http://hyperphysics.phy-astr.gsu.edu/hbase/nuclear/impar.html"

[24] Bremsstrahlung
"http://boojum.as.arizona.edu/~jill/A300b/Lectures/Bremsstrahlung.pdf"

[25] CMS Collaboration. Jet Energy Calibration and Transverse Momentum Resolution in CMS. 2011. CMS-PAS-JME-10-011.

[26] Michel Della Negra, L Fo'a, A Herve, and Achille Petrilli. CMS physics: Technical Design Report. CERN, Geneva, 2006.

[27] Torbjorn Sjostrand. Pythia 6.4 Physics and Manual. hep-ph/0603175, 2006.

[28] G. Corcella et al. HERWIG 6.5: an event generator for Hadron Emission Reactions With Interfering Gluons (including supersymmetric processes). JHEP, 01:010, 2001. hep-ph/0011363.

[29] Rikkert Frederix. Recent developments in madgraph/madevent v4. Nuclear Physics B - Proceedings Supplements, 183:285 289, 2008. Proceedings of the 9th DESY Workshop on Elementary Particle Theory.

[30] Simone Alioli, Paolo Nason, Carlo Oleari, and Emanuele Re. A general framework for implementing NLO calculations in shower Monte Carlo programs: the POWHEG BOX. JHEP, 06:043, 2010. arXiv:1002.2581.

[31] ROOT,
"`http://root.cern.ch/`".

[32] J. Allison et al. Geant4 developments and applications. Nuclear Science, IEEE Transactions on, 53(1):270 278, Feb. 2006.

[33] National Centre for Physics
"`http://www.ncp.edu.pk/`"

[34] PK-Grid-CA website
"`http://www.ncp.edu.pk/pk-grid-ca`"

[35] Baseline muon selections
"`https://twiki.cern.ch/twiki/bin/view/CMSPublic/SWGuideMuonId`"

[36] 2012 CMS Data Analysis School Pileup Reweighting Exercises
"`https://twiki.cern.ch/twiki/bin/view/CMS/SWGuideCMSDataAnalysisSchool2012PileupReweighting`"

[37] "`https://cms-service-dqm.web.cern.ch/cms-service-dqm/CAF/certification/Collisions12/`"

[38] W. M. Yao et al. Review of particle physics. J. Phys., G33:11232, 2006.

[39] namespace RooFit
"`http://root.cern.ch/root/html/RooFit.html`"

[40] Wolfram MathWorld
"`http://mathworld.wolfram.com/GaussianFunction.html`"

[41] Muon momentum scale corrections with MuScleFit (2011-2012 data and Monte Carlo) (PRELIMINARY)
"https://twiki.cern.ch/twiki/bin/view/CMSPublic/MuScleFitCorrections2012"

[42] /afs/cern.ch/user/s/scasasso/www/MuScleFit/$plots\_070413/DATAvsMC\_2012$
"https://scasasso.web.cern.ch/scasasso/MuScleFit/$plots_070413$/$DATAvsMC_2012$/"

[43] Measurement of inclusive W and Z boson cross section in pp collisions at center of mass energy of 8 TeV
CMS AN AN-12-067, CMS Draft Analysis Note, 29 June 2012